

A General Track Fit based on Triplets

A. Schöning^a

^a*Physics Institute, Heidelberg University, Im Neuenheimer Feld 226, 69120 Heidelberg, Germany*

Abstract

This work presents an analytical solution for a general three-dimensional track fit based on hit triplets. Input to the fit are triplet parameters, which contain information about the triplet geometry (hit positions), the radiation length of the material and the magnetic field. The general fit considers spatial hit and multiple Coulomb scattering uncertainties, and can also be extended to include energy losses.

The output of the fit, which is given by an analytical closed-form solution, contains the total momentum and the hit residuals, including the full covariance matrix, thus allowing for easy software alignment of the detector. The fit qualities are calculated for the global track fit as well as for the local hit triplets. This feature allows filtering out triplets with poor fit quality at an early stage of track reconstruction. The fit of local triplets is fully parallelizable, enabling accelerated computation with parallel hardware architectures.

The triplet track fit is detector-independent, making it possible to use the same fitting code for all tracking detectors. Only the detector-specific triplet parameters (fit input) depend on the triplet geometries and the magnetic field. Formulas for the calculation of the triplet parameters are given for the most common tracking detector setups, namely a homogeneous magnetic field and a spectrometer using a dipole magnet. Furthermore, an algorithm is presented to calculate tracking parameters for an arbitrary magnetic field configuration.

Moreover, this work includes a discussion of track fit biases and presents an extension of the fit to include energy losses. Last but not least, it is proposed to use triplet-based scale parameters that characterize different tracking regimes to accelerate track fits and to optimize the design of future tracking detectors.

Keywords: tracking, track fit, track fit bias, hit triplet, multiple scattering, fit quality, software alignment, spectrometer, energy loss, tracking regimes

1. Introduction

In nuclear and particle physics experiments, the precise determination of the track parameters for measuring charged particles is crucial. Therefore an accurate tracking model is required that takes into account all error sources of the measurement, the most relevant being hit position errors, multiple Coulomb scattering (MS), energy losses and magnetic field errors.

The most commonly used track fit today is the Kálmán filter [1, 2]. It uses a state vector to parameterize the track, which is updated with each measurement (hit), together with the track fit quality. The fit quality is the most important estimator in track reconstruction for finding the correct hit combinations. Especially in high-rate experiments, track finding is a major challenge due to large hit combinatorics. The use of a correct tracking model is therefore crucial for achieving a high track reconstruction efficiency. Nowadays, an extension of the Kálmán filter, the combinatorial Kálmán filter [3], is used in many experiments for track reconstruction.

The Kálmán filter, however, also has disadvantages: the Kálmán filter algorithm is sequential and iterative, and consequently not well suited for parallel computing. This

poses a severe limit for accelerating track reconstruction using modern computing models. In addition, the Kálmán filter cannot be used for detector alignment since the state vector does not provide the hit covariance matrix. Considering that detector resolutions continue to improve with new tracking detector technologies, the software alignment of the detector system becomes increasingly relevant to fully exploit the potential of detectors.

For this task, the General Broken Line (GBL) fit [4, 5] is ideal as it allows the calculation of the full hit covariance matrix required to determine the alignment constants [6, 7]. The basic concept of the GBL is to linearize an approximate solution and perform the track fit in a local (curvilinear) coordinate system defined by a reference (seed) solution. MS as well as energy losses then show up as kinks in the transformed trajectory. These kinks are minimized along with the hit residuals in the fit. As the GBL is seeded and requires an approximate solution as starting point, it cannot be used for track finding.

The MS triplet fit [8] is an alternative track fit that uses a linearization approach quite similar to the GBL but does not require any seed or approximate solution. Triplets of hits have the advantage that the reference trajectory for the linearization can be easily calculated from the triplet

geometry itself, for example in a homogeneous magnetic field. Furthermore, hit triplets are over-constrained, allowing the calculation of a triplet quality that can be used to reject fake hit combinations at an early stage of track reconstruction.

Because the result of a single triplet fit can be written as a simple function of triplet-specific parameters and the global track parameters can be calculated from simple sums of local triplet fits, the MS triplet fit is much faster than any other track fit. Its parallelization capability makes the MS triplet fit ideal for parallel computing, for example on graphics processing units (GPUs). However, since hit position uncertainties are not included, the MS triplet fit is restricted to low-momentum tracks, where MS errors are dominant. The MS triplet fit is used by the Mu3e experiment [9], which searches for the decay $\mu \rightarrow eee$ using muons decaying at rest. Here, the triplet fit has been implemented for both offline reconstruction [10] and online track reconstruction on a GPU-based event filter [11].

This work presents an extension of the MS triplet fit that takes into account also hit uncertainties as well as all correlations between different hit triplets. Therefore, this work goes beyond Ref.[12], where hit uncertainties were added only in the calculation of single triplet fit qualities, but correlations between different hit triplets were neglected. Interestingly, as will be shown in this work, the solution of the general triplet track fit, which includes both MS *and* hit position uncertainties, can also be given in an analytical closed-form solution.

A difference between the General Triplet Track Fit (GTTF) and other track fits is the fit input. The Kálmán filter and the GBL use hit positions as input. In contrast, the GTTF uses so-called *triplet parameters* as input, which represent an interface to all kind of tracking detectors and provide a general description of the detector (triplet) geometry, including the hit position uncertainties, the scattering material and the magnetic field. For this reason, the GTTF is universal as the same fitting code can be used for all tracking detectors and for all experiments. Only the triplet parameters are experiment- and triplet-specific.

The most important advantage of GTTF is the ability to perform triplet filtering during track reconstruction. This, together with the ability to perform track fitting of triplets on a parallel computer architecture, offers great potential for speeding up the track reconstruction in high particle rate experiments. In addition, the GTTF provides the hit covariance matrix, making it ideal for software alignment of tracking detectors.

Thanks to the analytical form of the result, it is also rather easy to calculate the tracking resolution for a given detector geometry without the need for extensive simulation studies. This feature greatly simplifies tracking detector design studies for future experiments.

With the triplet concept one can go even one step further; by calculating simple scale parameters based on triplets, *tracking regimes* can be defined. Depending on

the tracking regime, different numerical optimizations can be used to accelerate track fitting. Furthermore, a tracking regime analysis can also help in identifying weaknesses of tracking detector designs.

The paper is organized as follows. The fit methodology is introduced in Section 2. The formulas for the global triplet track fit are derived in Section 3, first for the general case and then in the limit of dominant hit position errors and dominant MS errors. Results for local triplet fits are given in Section 4. Track fits are in general biased if MS errors dominate; a detailed analysis of this bias as well as mitigation strategies, including an special regularized MS fit with reduced bias, is presented in Section 5. The triplet parameters, which represent the input to the fit, are calculated in Section 6; herein, analytical formulas are derived for triplets in a homogeneous magnetic field and for a spectrometer setup with an ideal dipole. Energy loss corrections and track fits including energy losses are discussed in Section 7. The potential for exploiting parallel computing for track fitting and track reconstruction using the triplet concept is presented in Section 8. Last but not least, characteristic tracking scale parameters are defined and the triplet-based tracking regime concept is introduced in Section 9. A summary is given in Section 10

2. Fit Methodology and Triplet Representation

The track fit aims at fitting the total particle momentum, p , and the hit positions by simultaneously minimising the MS angles and the hit position shifts. The hit positions are given as shifts with respect to the measured hit positions $\delta\vec{x}_k = \vec{x}_{\text{fit},k} - \vec{x}_{\text{meas},k}$, with k being the hit index. For a given magnetic field, this set of parameters (p and all $\delta\vec{x}_k$) contains the full information about the particle trajectory.

For track fitting, a χ^2 function is defined that includes MS as well as spatial hit uncertainties according to:

$$\chi^2 = \sum_{j=0}^{n_{\text{scat}}-1} \frac{\Delta\Theta_{\text{MS},j}^2}{\sigma_{\Theta_{\text{MS},j}}^2} + \sum_{j=0}^{n_{\text{scat}}-1} \frac{\Delta\Phi_{\text{MS},j}^2}{\sigma_{\Phi_{\text{MS},j}}^2} + \sum_{k=0}^{n_{\text{hit}}-1} \delta\vec{x}_k^t V_k^{-1} \delta\vec{x}_k. \quad (1)$$

The first two sums¹ run over all hit triplets (index j) and describe MS at the n_{scat} scattering points. Throughout the work, it is assumed that the position of the scatterers agree with the position of the hits (detector layers). Using spherical coordinates, the MS kink is described by polar ($\Delta\Theta_{\text{MS},j}$) and azimuthal ($\Delta\Phi_{\text{MS},j}$) angles. The projected MS angles are divided by the corresponding expected errors ($\sigma_{\Theta_{\text{MS},j}}$ and $\sigma_{\Phi_{\text{MS},j}}$). The third sum runs over all hits and describes the contribution from the hit position

¹Throughout this paper, counting of hits and triplets starts at 0.

shifts (residuals). For each hit, the spatial uncertainty is described by a 3×3 covariance matrix, V_k .

The kink angles in the MS terms of Equation 1 depend on the total particle momentum, as illustrated in Figure 1. Instead of the particle momentum, p , the 3D curvature, κ , is used in the following². Both quantities can be converted into each other using the relation

$$\kappa = \frac{qB}{p}. \quad (2)$$

Note that for an inhomogeneous magnetic field, $B = B(\vec{x})$, κ is position dependent even if total momentum is conserved.

Matter effects are described by two parameters, a MS parameter and an energy loss parameter. For each hit, both parameters are calculated from the effective path length in the tracking layer material. Note that both matter effects have some momentum (energy) dependence. The error of the MS angle, σ_{MS} , depends on the momentum and velocity of the particle [13, 14]. Assuming that the particle is ultra-relativistic ($v \approx c$), MS is inverse proportional to the 3D curvature

$$\sigma_{\text{MS}} \propto \frac{1}{|p|}, \quad (3)$$

and one can define a *MS parameter* according to:

$$b_{\text{MS}} = \frac{\sigma_{\text{MS}}}{|\kappa|} = \sigma_{\text{MS}} \left| \frac{p}{qB} \right|. \quad (4)$$

Similarly, an energy loss parameter, ΔE , is defined for each tracking layer (hit), accounting for the energy loss, for example due to ionization. An advantage of the triplet fit is that both, the momentum and the effective path length can already be derived from the triplet geometry before fitting (see Section 6).

In the following, it is assumed that the total momentum of the particles is conserved. Energy losses are included at a later stage and discussed in Section 7.

2.1. Triplet Parameters

Inside a magnetic field, the value of the total momentum defines³ the trajectory between two consecutive hits. Consequently, the total momentum defines the kink angle $\Delta\Psi = (\Delta\Theta, \Delta\Phi)$ for a hit triplet, as shown in Figure 1. Throughout this paper, a right-handed coordinate system is used, with the polar angle, θ , being defined with respect to the z -axis, and the azimuthal angle, ϕ , being defined with respect to the x -axis. The two projections of the kink angle at detector layer k are then defined as:

$$\Delta\Theta(p) = \Delta\Theta(\kappa) := \theta_{k,k-1} - \theta_{k,k+1}, \quad (5)$$

$$\Delta\Phi(p) = \Delta\Phi(\kappa) := \phi_{k,k-1} - \phi_{k,k+1}, \quad (6)$$

²In many other papers, κ is used to denote the transverse curvature, which is henceforth denoted as $\kappa_{\perp} = \frac{qB}{p_{\perp}}$ in this paper.

³Note that there might be no solution for low total momentum tracks, and more than one solution for high momentum tracks, depending on the field configuration.

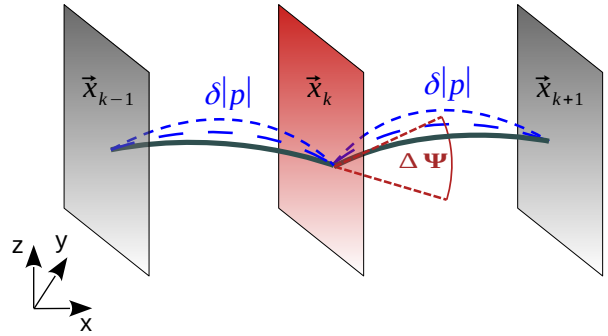


Figure 1: Sketch of a hit triplet illustrating the kink angle $\Delta\Psi = (\Delta\Theta, \Delta\Phi)$ at the scattering layer k and the change of the trajectory for a variation of the total momentum.

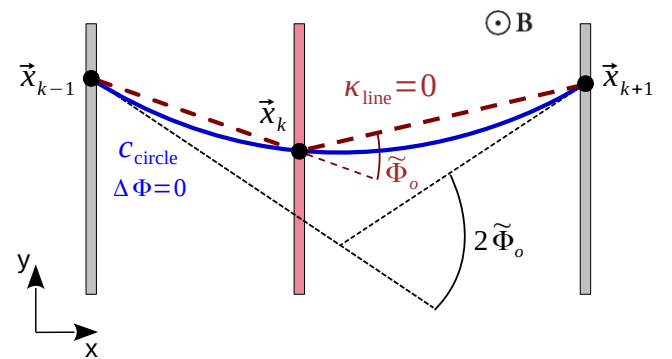


Figure 2: Sketch of a hit triplet in the bending plane of an homogeneous magnetic field. The *blue solid line* shows the solution for $\Delta\Phi = 0$ (zero kink angle); the *brown dashed line* the zero curvature solution ($\kappa = 0$). The triplet parameter $\tilde{\Phi}_0$ corresponds to the kink angle of the zero curvature solution. The bending angle, Φ , of the zero kink angle solution is related to the kink angle of the zero curvature solution via $\Phi(\Delta\Phi=0) = 2\tilde{\Phi}_0$.

where the subscript “ $k, k - 1$ ” (“ $k, k + 1$ ”) indicates the particle direction at the detector plane before (after) the scattering process. Both kink angles are a function of the momentum (\cong 3D curvature). For typical tracking detectors, these functions are transcendental. This is, for example, the case for tracking in a homogeneous magnetic field or a spectrometer setup. Both cases are discussed in Section 6.

A method for solving the (transcendental) functions $\Theta(\kappa)$ and $\Phi(\kappa)$ is to perform a linearization around a known solution. Throughout the paper, the solution

$$\Phi_{\text{ref}} := \Phi(\kappa_{\text{ref}}) = 0 \quad (7)$$

is used as *reference trajectory*, corresponding to no MS in the x - y plane, which is defined to be the *main bending plane*. The reference solution is described by the 3D curvature, κ_{ref} , and has a non-vanishing polar kink angle $\Theta_{\text{ref}} := \Theta(\kappa_{\text{ref}})$, in general. The first order linearization

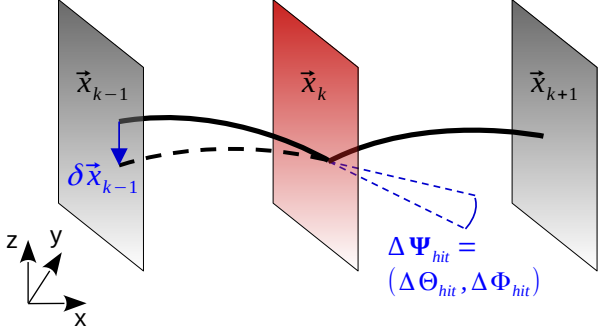


Figure 3: Sketch of a hit triplet illustrating the kink angle variation $\Delta\Theta_{hit}$ and $\Delta\Phi_{hit}$ at the scattering layer k for a variation of the hit position in layer $k-1$.

around the reference solution then reads:

$$\Delta\Phi = 0 + (\kappa - \kappa_{ref})\rho_\Phi + O(\kappa^2) \approx \tilde{\Phi}_0 + \rho_\Phi \kappa, \quad (8)$$

$$\Delta\Theta = \Theta_{ref} + (\kappa - \kappa_{ref})\rho_\Theta + O(\kappa^2) \approx \tilde{\Theta}_0 + \rho_\Theta \kappa. \quad (9)$$

The same ansatz was already used in Ref.[8], with the only difference that the linearization was done as function of the 3D radius $R_{3D} = \kappa^{-1}$, leading to marginally different numerical results for MS fits.

The four linearization parameters $\tilde{\Phi}_0$, $\tilde{\Theta}_0$, ρ_Φ and ρ_Θ are *fundamental* parameters, which describe the curvature dependence of the triplet kink angles. In the small bending limit, $\kappa \rightarrow 0$, the fundamental triplet parameters $\tilde{\Phi}_0$ and $\tilde{\Theta}_0$ can be interpreted as central angle of the hit triplet (see Figure 2 for $\tilde{\Phi}_0$). The parameter ρ_Φ is always negative and its absolute value can be interpreted as effective arc lengths of the triplet, as will be shown in Section 6. The parameter ρ_Θ is a small correction factor and has no simple geometrical interpretation.

The hit position uncertainties in Equation 1 are given in global coordinates. Without loss of generality, a transformation $\vec{x}_k \rightarrow \vec{x}'_k$ into local hit coordinates is possible such that the corresponding hit covariance matrix $V_k'^{-1}$ becomes diagonal. For each hit, therefore, a local coordinate system with the orthogonal base $(\vec{u}_k, \vec{v}_k, \vec{w}_k)$ can be defined. To describe the residuals in the three orthogonal directions, the vector

$$\vec{\delta}_k := (\delta_{k,u_k}, \delta_{k,v_k}, \delta_{k,w_k})^t \quad (10)$$

is defined. The corresponding (diagonal) covariance matrix then reads as follows:

$$\text{Cov}_{\delta,k} := V_k'^{-1} = \text{diag}(\sigma_{k,u}^2, \sigma_{k,v}^2, \sigma_{k,w}^2), \quad (11)$$

with $\sigma_{k,i}$ being the hit position uncertainties in the i^{th} direction.

2.2. Representation of Hit Position Uncertainties

The variation of a hit position leads to a change of the kink angles as shown in Figure 3. In practically all tracking devices the hit position uncertainties are much

smaller than the distance between hits and tracking layers, i.e., $\text{Tr}(\text{Cov}_{\delta,k}) \ll \rho_\Phi^2$. Since the fit of the hit positions only slightly changes the triplet kink angles, the hit position-induced kinks are parameterized using the linearization ansatz:

$$\Delta\Theta_{hit} = \sum_{k=0}^2 \vec{h}_{\Theta_k} \vec{\delta}_k, \quad (12)$$

$$\Delta\Phi_{hit} = \sum_{k=0}^2 \vec{h}_{\Phi_k} \vec{\delta}_k, \quad (13)$$

with \vec{h}_{Φ_k} and \vec{h}_{Θ_k} being three vectors defined as directional gradients of the three hit positions:

$$\vec{h}_{\Theta_k} = \vec{\nabla}_{\vec{\delta}_k} \tilde{\Theta}(\vec{x}_k), \quad (14)$$

$$\vec{h}_{\Phi_k} = \vec{\nabla}_{\vec{\delta}_k} \tilde{\Phi}(\vec{x}_k). \quad (15)$$

The directional hit gradients can, for instance, numerically be determined by re-calculating the kink angles, $\Delta\Theta$ and $\Delta\Phi$, after variation of the three hit positions, for example by shifting the hits by 1-sigma of the hit position error into the three orthogonal directions⁴. An alternative method based on track extrapolations is discussed in the context of inhomogeneous magnetic fields in Section D.3.

Finally, the MS angles of a triplet entering Equation 1 are expressed as function of the four fundamental triplet parameters, the 3D curvature and the hit position-induced kinks:

$$\Theta_{MS} = \tilde{\Theta} + \rho_\Theta \kappa - \Delta\Theta_{hit} \quad (16)$$

$$\Phi_{MS} = \tilde{\Phi} + \rho_\Phi \kappa - \Delta\Phi_{hit}. \quad (17)$$

For the general fit of a single triplet, a total of 23 parameters are required. These are the four fundamental triplet parameters, the 3×3 components of the hit gradients, the corresponding hit position uncertainties, and one material parameter. The number of parameters reduces to five for MS fits where hit uncertainties are neglected.

3. Global Triplet Track Fit

Using the triplet parameters and the local hit coordinate representation introduced in the last section, the χ^2 function (Equation 1) can be re-written as:

$$\begin{aligned} \chi^2(\kappa, \vec{\delta}) = & \sum_{j=0}^{n_{hit}-3} \frac{(\tilde{\Theta}_j + \rho_\Theta \kappa - \Delta\Theta_{hit,j}(\vec{\delta}))^2}{\sigma_{\tilde{\Theta}_{MS,j}}^2} \\ & + \sum_{j=0}^{n_{hit}-3} \frac{(\tilde{\Phi}_j + \rho_\Phi \kappa - \Delta\Phi_{hit,j}(\vec{\delta}))^2}{\sigma_{\tilde{\Phi}_{MS,j}}^2} \\ & + \sum_{k=0}^{n_{hit}-1} \vec{\delta}_k^t \text{Cov}_{\delta,k}^{-1} \vec{\delta}_k. \end{aligned} \quad (18)$$

⁴Note that the components of the vectors \vec{h} and $\vec{\delta}_k$ refer to the base of the local coordinates and not to the global coordinate system.

The fit parameters are the 3D curvature, κ , and the residuals⁵ $\vec{\delta} = (\vec{\delta}_0, \vec{\delta}_1, \dots, \vec{\delta}_{n_{\text{hit}}-1})^\top$. The 3D curvature, κ is here defined with respect to a reference magnetic field, according to:

$$\frac{q}{p} = \frac{\kappa}{B_{\text{ref}}} = \frac{\kappa_j}{B_j}, \quad (19)$$

with B_j being the local magnetic field strengths at triplet j and B_{ref} being a reference magnetic field. Note that for inhomogeneous magnetic fields, the field dependence of κ can be “absorbed” by the ρ coefficients in Equation 18 by replacing: $\rho_j \rightarrow \rho_j B_{\text{ref}}/B_j$.

The momentum dependence of the scattering uncertainty is purposely⁶ neglected in Equation 18, in order to have at most quadratic terms as function of κ and $\vec{\delta}$. To bring Equation 18 in a more legible form, it is convenient to define two fundamental triplet parameter vectors:

$$\begin{aligned} \boldsymbol{\rho} &= (\rho_{\Theta_0}, \dots, \rho_{\Theta_{n_{\text{hit}}-3}}; \rho_{\Phi_0}, \dots, \rho_{\Phi_{n_{\text{hit}}-3}})^\top, \\ \vec{\Psi} &= (\tilde{\Theta}_0, \dots, \tilde{\Theta}_{n_{\text{hit}}-3}; \tilde{\Phi}_0, \dots, \tilde{\Phi}_{n_{\text{hit}}-3})^\top, \end{aligned}$$

whose length is twice the number of triplets. Moreover, *precision matrices* are defined for MS and hit position errors:

$$\begin{aligned} \mathbf{D}_{\text{MS}} &= \text{diag} \left(\frac{1}{\sigma_{\Theta_{\text{MS},0}}^2}, \dots, \frac{1}{\sigma_{\Theta_{\text{MS},n_{\text{hit}}-3}}^2}; \right. \\ &\quad \left. \frac{1}{\sigma_{\Phi_{\text{MS},0}}^2}, \dots, \frac{1}{\sigma_{\Phi_{\text{MS},n_{\text{hit}}-3}}^2} \right), \\ \vec{\vec{D}}_{\text{hit}} &= \text{diag} \left(\text{Cov}_{\delta,0}^{-1}, \text{Cov}_{\delta,1}^{-1}, \dots, \text{Cov}_{\delta,n_{\text{hit}}-1}^{-1} \right). \end{aligned}$$

\mathbf{D}_{MS} and $\vec{\vec{D}}_{\text{hit}}$ are diagonal matrices, whose ranks are $2n_{\text{triplet}}$ and $3n_{\text{hits}}$, respectively. The rank of \mathbf{D}_{MS} corresponds to the number of triplets. Elements in the MS precision matrix \mathbf{D}_{MS} are partially related, since:

$$\sigma_{\Theta_{\text{MS},j}} = \sigma_{\text{MS},j}, \quad (20)$$

$$\sigma_{\Phi_{\text{MS},j}} = \sigma_{\text{MS},j} / \sin \hat{\vartheta}_j, \quad (21)$$

with $\sigma_{\text{MS},j}$ being the MS angular error (Equation 3) of the j^{th} triplet and $\hat{\vartheta}_j$ being the corresponding estimated average polar angle in the MS process. Note that the $1/\sin \hat{\vartheta}_j$ factor in Equation 21 is a geometrical factor originating from the spherical coordinate representation.

⁵Here (and in the following), bold symbols refer to vectors (lowercase variables) and matrices (uppercase variables), either in hit or triplet space. Furthermore, within this work two different transposition signs are used. The t operator acts on Euclidean space, whereas the $^\top$ operator acts on both triplet space and hit space, also including all directions of the hit position errors.

⁶Neglecting the momentum dependence in Equation 3 by setting σ_{MS} constant, leads to a small momentum bias in the fit for MS-dominated particles that, however, can be corrected (see Section 5).

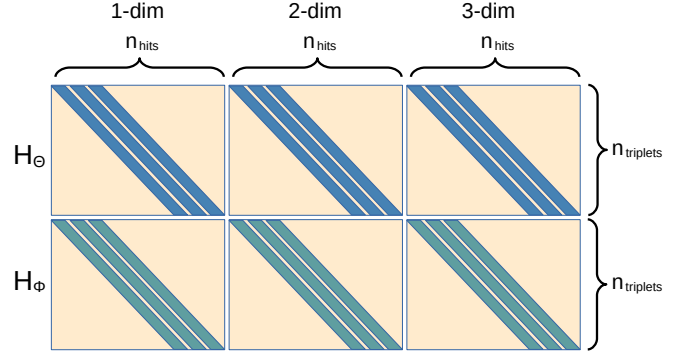


Figure 4: Sketch of the rectangular matrix \vec{H} . The horizontal block structure originates from the three orthogonal hit position uncertainties directions. The vertical block structure originates from the two projections of the MS angular error. Only elements in the blue and turquoise bands are non-zero.

The hit gradients can be all collected by defining hit space vectors for each hit triplet:

$$\begin{aligned} \vec{h}_{\Theta,j} &=: (\vec{h}_{\Theta_0}^{(j)}, \vec{h}_{\Theta_1}^{(j)}, \dots, \vec{h}_{\Theta_{n_{\text{hit}}-1}}^{(j)}), \\ \vec{h}_{\Phi,j} &=: (\vec{h}_{\Phi_0}^{(j)}, \vec{h}_{\Phi_1}^{(j)}, \dots, \vec{h}_{\Phi_{n_{\text{hit}}-1}}^{(j)}). \end{aligned}$$

Only the elements with the indices j , $j+1$ and $j+2$ are non-zero. These hit gradient vectors, defined for each triplet, can be written in compact matrix form as:

$$\vec{H} = \begin{pmatrix} \vec{h}_{\Theta,0}, \dots, \vec{h}_{\Theta,n_{\text{hit}}-3}; \\ \vec{h}_{\Phi,0}, \dots, \vec{h}_{\Phi,n_{\text{hit}}-3} \end{pmatrix}^\top.$$

The hit gradient matrix (Jacobian) has in total $2n_{\text{triplet}} \times 3n_{\text{hit}}$ components; its structure is sketched in Figure 4.

The χ^2 function (Equation 18) then reads in compact form:

$$\chi^2(\kappa, \vec{\delta}) = \left(\boldsymbol{\Psi} + \boldsymbol{\rho} \kappa - \vec{H} \vec{\delta} \right)^\top \mathbf{D}_{\text{MS}} \left(\boldsymbol{\Psi} + \boldsymbol{\rho} \kappa - \vec{H} \vec{\delta} \right) + \vec{\delta}^\top \vec{\vec{D}}_{\text{hit}} \vec{\delta}. \quad (22)$$

Minimising Equation 22 results in a system of linear equations:

$$\begin{pmatrix} -\boldsymbol{\rho}^\top \mathbf{D}_{\text{MS}} \vec{\Psi} \\ \vec{H}^\top \mathbf{D}_{\text{MS}} \vec{\Psi} \end{pmatrix} = \begin{pmatrix} \boldsymbol{\rho}^\top \mathbf{D}_{\text{MS}} \boldsymbol{\rho} & -\boldsymbol{\rho}^\top \mathbf{D}_{\text{MS}} \vec{H} \\ -\vec{H}^\top \mathbf{D}_{\text{MS}} \boldsymbol{\rho} & \vec{\vec{D}}_{\text{hit}} + \vec{H}^\top \mathbf{D}_{\text{MS}} \vec{H} \end{pmatrix} \begin{pmatrix} \kappa \\ \vec{\delta} \end{pmatrix}. \quad (23)$$

Solving the system above yields for the 3D curvature and its variance:

$$\kappa_{\text{min}} = -\frac{\boldsymbol{\rho}^\top \mathbf{K} \boldsymbol{\Psi}}{\boldsymbol{\rho}^\top \mathbf{K} \boldsymbol{\rho}}, \quad (24)$$

$$\sigma_{\kappa_{\text{min}}}^2 = \frac{1}{\boldsymbol{\rho}^\top \mathbf{K} \boldsymbol{\rho}}, \quad (25)$$

with \mathbf{K} being the *triplet precision matrix*. Its inverse, the covariance matrix, is defined as:

$$\mathbf{K}^{-1} = \mathbf{D}_{\text{MS}}^{-1} + \vec{\mathbf{H}} \vec{\mathbf{D}}_{\text{hit}}^{-1} \vec{\mathbf{H}}^{\top}. \quad (26)$$

\mathbf{K}^{-1} combines the MS and hit position covariance matrices and is called *triplet covariance matrix*. Inversion of the triplet covariance matrix is trivial in case of dominant MS errors since $\mathbf{D}_{\text{MS}}^{-1}$ is diagonal (see also Section 3.2). The inversion is more involved if spatial hit uncertainties contribute. Note that the matrix $\vec{\mathbf{H}} \vec{\mathbf{D}}_{\text{hit}}^{-1} \vec{\mathbf{H}}^{\top}$ has a 2×2 block structure with penta-diagonal sub-matrices.⁷

The residuals and the corresponding covariance matrix are calculated as:

$$\vec{\delta}_{\text{min}} = \vec{\mathbf{D}}_{\text{hit}}^{-1} \vec{\mathbf{H}}^{\top} \mathbf{K}_{\rho} \Psi, \quad (27)$$

$$\text{Cov}_{\delta_{\text{min}}} = \vec{\mathbf{D}}_{\text{hit}}^{-1} - \vec{\mathbf{D}}_{\text{hit}}^{-1} \vec{\mathbf{H}}^{\top} \mathbf{K}_{\rho} \vec{\mathbf{H}} \vec{\mathbf{D}}_{\text{hit}}^{-1}, \quad (28)$$

with

$$\mathbf{K}_{\rho} = \left(\mathbf{K} - \frac{\mathbf{K} \rho \rho^{\top} \mathbf{K}}{\rho^{\top} \mathbf{K} \rho} \right). \quad (29)$$

Note that the matrix \mathbf{K}_{ρ} only exists for $\det(\mathbf{K}) \neq 0$.

Finally, the fit quality is given by:

$$\begin{aligned} \chi_{\text{min}}^2 &= \Psi^{\top} \mathbf{K} \Psi - \frac{(\rho^{\top} \mathbf{K} \Psi)^2}{\rho^{\top} \mathbf{K} \rho} \\ &= \Psi^{\top} \mathbf{K}_{\rho} \Psi. \end{aligned} \quad (30)$$

In the first line, the first term accounts for the kink angles of the infinite momentum solution whereas the second term describes the improvement of the fit quality by fitting the hit positions and the 3D curvature. The second line of Equation 30 suggests that the matrix \mathbf{K}_{ρ} can be interpreted as post-fit precision matrix for the kink angles.

In the fit described above, all triplet parameters are treated as constants. This approach is valid if MS errors and hit position errors are small. The fit accuracy is given by the norm of the triplet covariance matrix $\|\mathbf{K}^{-1}\|$. For large values of this norm, rotational uncertainties of triplets should be considered, which have not been considered so far. For strip detectors, which have a large uncertainty in one direction, the rotational uncertainties are given in Appendix E.

3.1. Global Fit for Dominant Hit Position Errors

In the limit of dominating hit position uncertainties, the MS errors vanish: $\|\mathbf{D}_{\text{MS}}\|^{-1} \rightarrow 0$. The solution for this case looks similar to the general case (previous section), and is given in Appendix A, for completeness.

⁷The penta-diagonal structure of the sub-matrices can be exploited for large matrices where the computational effort for the inversion scales linearly with the number of hits (tracking layers).

3.2. Global Fit for Dominant MS Errors

In the case of dominant MS errors, the hit positions uncertainties vanish. By replacing the triplet covariance matrix by the MS covariance matrix, $\mathbf{K} \rightarrow \mathbf{D}_{\text{MS}}$, one obtains for the curvature and its variance:

$$\kappa_{\text{MS}} = -\frac{\rho^{\top} \mathbf{D}_{\text{MS}} \Psi}{\rho^{\top} \mathbf{D}_{\text{MS}} \rho}, \quad (31)$$

$$\sigma_{\kappa_{\text{MS}}}^2 = \frac{1}{\rho^{\top} \mathbf{D}_{\text{MS}} \rho}, \quad (32)$$

and for the fit quality:

$$\chi_{\text{MS}}^2 = \Psi^{\top} \mathbf{D}_{\text{MS}} \Psi - \frac{(\rho^{\top} \mathbf{D}_{\text{MS}} \Psi)^2}{\rho^{\top} \mathbf{D}_{\text{MS}} \rho}. \quad (33)$$

Due to the diagonal form of \mathbf{D}_{MS} , the global curvature and the fit quality can be written as simple error-weighted sums of local triplet quantities:

$$\kappa_{\text{MS}} = \sigma_{\kappa_{\text{MS}}}^2 \sum_{j=0}^{n_{\text{triplet}}-1} \frac{\kappa_{\text{MS},j}^2}{\sigma_{\kappa_{\text{MS},j}}^2}, \quad (34)$$

$$\frac{1}{\sigma_{\kappa_{\text{MS}}}^2} = \sum_{j=0}^{n_{\text{triplet}}-1} \frac{1}{\sigma_{\kappa_{\text{MS},j}}^2}, \quad (35)$$

$$\chi_{\text{MS}}^2 = \sum_{j=0}^{n_{\text{triplet}}-1} \chi_{\text{MS},j}^2 + \sum_{j=0}^{n_{\text{triplet}}-1} \frac{(\kappa_{\text{MS}} - \kappa_{\text{MS},j})^2}{\sigma_{\kappa_{\text{MS},j}}^2}, \quad (36)$$

where the indexed parameters denote the results obtained from the local triplet fits, which can be given in analytical closed-form (see Section 4). Note that the fit quality (Equation 36) has two terms: a sum over the individual triplet qualities and a weighted sum over the curvature residuals (curvature consistency term⁸).

Fit Quality Relations

For dominant MS errors, the following inequality can be derived from Equation 36:

$$\chi_{\text{MS}}^2 \geq \sum_{j=0}^{n_{\text{triplet}}-1} \chi_{\text{MS},j}^2. \quad (37)$$

This inequality can be used to accelerate track reconstruction. Since the sum of the fit qualities of individual triplets gives an upper limit on the global track fit quality, Equation 37 can be used to positively identify tracks just by using information obtained at triplet level.

The fit quality of the MS fit is also related to the general fit quality:

$$\chi_{\text{min}}^2 = \chi_{\text{MS}}^2 + \frac{(\kappa_{\text{min}} - \kappa_{\text{MS}})^2}{\sigma_{\kappa_{\text{MS}}}^2} - \vec{\delta}_{\text{min}}^{\top} \vec{\mathbf{P}} \vec{\delta}_{\text{min}}, \quad (38)$$

⁸The combination of triplets using the MS fit was first discussed in Ref.[8] where, however, the curvature consistency term (Equation 39 therein) is not given.

with

$$\vec{P} = \vec{H}^\top D_{\text{MS}} \vec{H} + \vec{D}_{\text{hit}} \quad (39)$$

being the *adjoint triplet precision matrix*⁹, which has the rank $3n_{\text{hit}}$. The MS fit quality therefore poses an upper limit for the general fit quality:

$$\chi_{\text{min}}^2 \leq \chi_{\text{MS}}^2. \quad (40)$$

This relation is of high relevance for fast track finding. Since the computational effort for the MS fit is significantly lower than for the general fit, it is advantageous to perform the MS fit first and only use the general fit if necessary, for example for track candidates with dominant hit position uncertainties at high momentum.

4. Local Triplet Fit

The local triplet fit solution is readily obtained from Equations 24 to 30. For a single hit triplet, the triplet covariance matrix reduces to a 2×2 matrix. The elements of this local covariance matrix, defined as

$$\mathbf{K}_{\text{loc}}^{-1} = \begin{pmatrix} \Gamma_{\Theta\Theta}^* & \Gamma_{\Theta\Phi} \\ \Gamma_{\Theta\Phi}^* & \Gamma_{\Phi\Phi}^* \end{pmatrix}, \quad (41)$$

are given by:

$$\begin{aligned} \Gamma_{\Theta\Theta}^* &:= \Gamma_{\Theta\Theta} + \sigma_{\Theta_{MS}}^2 \\ &:= \sum_{k \in \text{triplet}} (\vec{h}_{\Theta_k} \vec{\sigma}_k)^2 + \sigma_{\Theta_{MS}}^2, \end{aligned} \quad (42)$$

$$\begin{aligned} \Gamma_{\Phi\Phi}^* &:= \Gamma_{\Phi\Phi} + \sigma_{\Phi_{MS}}^2 \\ &:= \sum_{k \in \text{triplet}} (\vec{h}_{\Phi_k} \vec{\sigma}_k)^2 + \sigma_{\Phi_{MS}}^2, \end{aligned} \quad (43)$$

$$\Gamma_{\Theta\Phi} := \sum_{k \in \text{triplet}} (\vec{h}_{\Theta_k} \vec{\sigma}_k) (\vec{h}_{\Phi_k} \vec{\sigma}_k). \quad (44)$$

The solution of the local triplet fit is a function of those Γ parameters. For the general fit, which includes MS and hit position errors, the 3D curvature and its variance are given by:

$$\begin{aligned} \kappa_{\text{loc}} &= \\ &- \frac{\tilde{\Theta}_0 \rho_\Theta \Gamma_{\Phi\Phi}^* + \tilde{\Phi}_0 \rho_\Phi \Gamma_{\Theta\Theta}^* - \Gamma_{\Theta\Phi} (\tilde{\Phi}_0 \rho_\Theta + \tilde{\Theta}_0 \rho_\Phi)}{\rho_\Theta^2 \Gamma_{\Phi\Phi}^* + \rho_\Phi^2 \Gamma_{\Theta\Theta}^* - 2\rho_\Theta \rho_\Phi \Gamma_{\Theta\Phi}}, \end{aligned} \quad (45)$$

$$\sigma_{\kappa_{\text{loc}}}^2 = \frac{\Gamma_{\Theta\Theta}^* \Gamma_{\Phi\Phi}^* - \Gamma_{\Theta\Phi}^2}{\rho_\Theta^2 \Gamma_{\Phi\Phi}^* + \rho_\Phi^2 \Gamma_{\Theta\Theta}^* - 2\rho_\Theta \rho_\Phi \Gamma_{\Theta\Phi}}. \quad (46)$$

For the local fit quality, one obtains:

$$\chi_{\text{loc}}^2 = \frac{(\tilde{\Theta}_0 \rho_\Phi - \tilde{\Phi}_0 \rho_\Theta)^2}{\rho_\Theta^2 \Gamma_{\Phi\Phi}^* + \rho_\Phi^2 \Gamma_{\Theta\Theta}^* - 2\rho_\Theta \rho_\Phi \Gamma_{\Theta\Phi}}. \quad (47)$$

⁹The triplet precision matrix and the adjoint triplet precision matrix are related by: $\vec{P}^{-1} \vec{H}^\top D_{\text{MS}} = \vec{D}_{\text{hit}}^{-1} \vec{H}^\top \mathbf{K}$.

Furthermore, the residual of hit k in direction i is given by:

$$\delta_{k_i, \text{loc}} = \sigma_{k_i}^2 \frac{(\rho_\Theta h_{\Phi k_i} - \rho_\Phi h_{\Theta k_i})}{(\rho_\Theta \tilde{\Phi}_0 - \rho_\Phi \tilde{\Theta}_0)} \chi_{\text{loc}}^2. \quad (48)$$

By exploiting Equation 47 and Equation 48, the hit covariance matrix of a single triplet can be given as function of the residuals in a simple form:

$$\mathbf{Cov}_\delta = \vec{D}_{\text{hit}}^{-1} - \frac{\vec{\delta}_{\text{loc}} \vec{\delta}_{\text{loc}}^\top}{\chi^2}. \quad (49)$$

The first term in Equation 49 contains the pre-fit hit position errors, whereas the second term describes their improvement by the track fit.

Special Cases for Local Triplet Fits

In the case of dominant hit position or MS errors, the local triplet fit (Equation 45 to Equation 47) further simplifies.

For dominant hit position errors, the following substitutions are possible:

$$\Gamma_{\Theta\Theta}^* \rightarrow \Gamma_{\Theta\Theta}, \quad (50)$$

$$\Gamma_{\Phi\Phi}^* \rightarrow \Gamma_{\Phi\Phi}. \quad (51)$$

For dominant MS errors, the following substitutions are possible:

$$\Gamma_{\Theta\Theta}^* \rightarrow \sigma_{\Theta_{MS}}^2 \quad (52)$$

$$\Gamma_{\Phi\Phi}^* \rightarrow \sigma_{\Phi_{MS}}^2 \quad (53)$$

$$\Gamma_{\Theta\Phi} \rightarrow 0. \quad (54)$$

For this case the residuals, given by Equation 48, vanish by definition. The 3D curvature (Equation 45 then simplifies to:

$$\kappa_{\text{MS}} = - \frac{\rho_\Phi \tilde{\Phi}_0 \sin^2 \hat{\vartheta} + \rho_\Theta \tilde{\Theta}_0}{\rho_\Phi^2 \sin^2 \hat{\vartheta} + \rho_\Theta^2}, \quad (55)$$

and becomes independent of the angular MS error. Unlike the GTTF (Equation 45), no curvature-dependent estimate of the MS uncertainty is needed as input to the local MS fit. However, the fit is not free of a bias, as discussed in the next section.

5. Curvature Bias in Track Fits

In the case of non-negligible MS errors, fits of the curvature and its error can be biased. The reason is that the MS angular errors ($\sigma_{\Theta_{\text{MS}}}$ and $\sigma_{\Phi_{\text{MS}}}$) are smaller for high momentum tracks than for low-momentum tracks; consequently, a bias is introduced if this momentum dependence is not included in the track fit. This bias occurs in all track fits.

5.1. Curvature Pull Distribution

One method to check the goodness of a fit is the study of pull distributions. The curvature pull for fit i is defined as:

$$g_{\kappa,i} = \frac{\kappa_i - \kappa^{\text{true}}}{\sigma_{\kappa,i}}. \quad (56)$$

For a fit with statistically correct estimates of κ and σ_{κ} , the arithmetic mean of the pull distribution is expected to vanish, $\mathbb{E}[g_{\kappa}] = 0$, and the variance is expected to be unity, $\text{Var}[g_{\kappa}] = 1$. In the following, the pull distribution is studied for the Local Track Fit and the Global Track Fit in a scenario where MS errors dominate.

5.1.1. Curvature Pull in the Local Track Fit

For a single triplet, the curvature pull can be calculated by smearing the particle momentum with a Gaussian distribution and recalculating the curvature error from the smeared quantity. One then obtains the result that the mean curvature pull is shifted towards smaller curvatures (higher momenta) and that the shift is given by:

$$\mathbb{E}[g_{\kappa}] \approx -\frac{|\sigma_{\kappa_{\text{MS}}}|}{\kappa}. \quad (57)$$

This result is valid if the curvature error is small compared to the curvature, i.e., $\sigma_{\kappa}^2 \ll \kappa^2$. Note that the curvature itself is correctly fitted, i.e., $\mathbb{E}[\kappa] = \kappa^{\text{true}}$. Since the bias of the curvature pull distribution is caused by the discarded momentum dependence of the MS angular error, this effect is henceforth referred to as *MS normalization bias*.

5.1.2. Curvature Pull in Global Triplet Track Fit

For dominant MS angular errors, the 3D curvature in the global fit becomes a weighted sum of the local triplet fits (see Section 3.2). Due to the MS normalization bias discussed in the previous section, high momentum triplets receive a higher weight in the fit than low-momentum triplets. This leads to the so-called *weighting bias* of the curvature.

For demonstration, the weighting bias has been studied for a simple detector geometry with n triplets with equidistant tracking layers. Using a toy Monte Carlo, the following relation was empirically found for the weighting bias:

$$\mathbb{E}[\kappa] - \kappa^{\text{true}} = -\frac{2n-2}{n} \frac{\sigma_{\kappa_{\text{MS}}}^2}{\kappa^{\text{true}}}. \quad (58)$$

The curvature bias therefore depends quadratically on the curvature error.

All together, the pull distribution (Equation 56) is influenced by two effects: the weighting bias, which leads to a shift in the curvature, and the MS normalization bias, which creates an asymmetry in the pull distribution.

5.2. Bias Mitigation in the Global Triplet Fit

The size of the bias depends on the accuracy with which the MS uncertainties are known prior to the fit. For the global fit, there are three ways to calculate the MS angular errors that enter the MS precision matrix \mathbf{D}_{MS} . With increasing precision, these are:

- from triplet parameter based estimates of the curvature (momentum), for example using the simple relation: $\kappa^{\text{est}} = \tilde{\Phi}_0 / \rho_{\Phi}$,
- from locally fitted curvatures derived before the global fit, $\kappa^{\text{est}} = \kappa_{\text{loc}}$ (Equation 45),
- by repeating the global fit (Equation 24 or Equation 31), where the MS angular errors are calculated from the curvature obtained in the first fit: $\kappa^{\text{est}} = \kappa(1^{\text{st}} \text{ fit})$.

Since the global fit has a significantly higher precision than the local fits, the bias is significantly reduced by using the third method. The downside is, however, that the precision matrix \mathbf{K} must be inverted again after updating the MS angular errors, essentially doubling the computational effort.

5.3. Regularized MS Fit

The curvature bias can be reduced by including the momentum dependence of the MS angular errors (Equation 3) in the fit. If included in the general fit formula (Equation 18), the minimization yields a system of equations that contains non-linear $\kappa^2 \cdot \delta_k$ terms, which is difficult to solve. However, since the bias is mainly relevant for the case of prevailing MS errors, the difficulty can be overcome by neglecting the hit position errors, such that the $\kappa^2 \cdot \delta_k$ terms vanish. The MS precision matrix can then be replaced by a new matrix that contains only the MS parameters defined in Equation 4, i.e.,

$$\mathbf{D}_{\text{MS}} \rightarrow \frac{1}{\kappa^2} \mathbf{B}_{\text{MS}}, \quad \text{with}$$

$$\mathbf{B}_{\text{MS}} := \text{diag} \left(\frac{1}{b_{\text{MS},0}^2}, \dots, \frac{1}{b_{\text{MS},n_{\text{hit}}-3}^2}; \frac{\sin^2 \hat{\vartheta}_0}{b_{\text{MS},0}^2}, \dots, \frac{\sin^2 \hat{\vartheta}_{n_{\text{hit}}-3}}{b_{\text{MS},n_{\text{hit}}-3}^2} \right).$$

The fit quality after linearization then reads in compact form:

$$\chi_{\text{MSreg}}^2(\kappa) = \frac{(\Psi + \rho \kappa)^{\top} \mathbf{B}_{\text{MS}} (\Psi + \rho \kappa)}{\kappa^2}. \quad (59)$$

Minimization of above equation yields:

$$\kappa_{\text{MSreg}} = -\frac{\Psi^{\top} \mathbf{B}_{\text{MS}} \Psi}{\rho^{\top} \mathbf{B}_{\text{MS}} \Psi}, \quad (60)$$

$$\sigma_{\kappa_{\text{MSreg}}}^2 = \frac{(\Psi^{\top} \mathbf{B}_{\text{MS}} \Psi)^3}{(\rho^{\top} \mathbf{B}_{\text{MS}} \Psi)^4}. \quad (61)$$

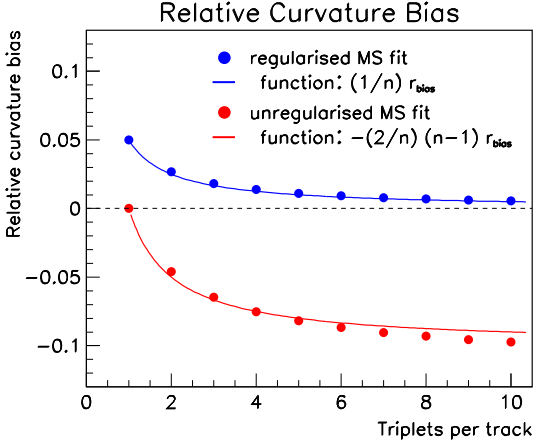


Figure 5: Simulated curvature bias (*circles*) as a function of the number of triplets per track for a relative curvature (momentum) resolution of 23%. The results are shown for regularized (*blue*) and unregularized (*red*) triplet fits. The statistical errors are of the order of 1 per mil. The data points are compared with empirical functions obtained from the simulation. See text for more explanation.

Finally, the fit quality is given by:

$$\chi_{\text{MSreg}}^2 = \boldsymbol{\rho}^\top \mathbf{B}_{\text{MS}} \boldsymbol{\rho} - \frac{(\boldsymbol{\rho}^\top \mathbf{B}_{\text{MS}} \boldsymbol{\Psi})^2}{\boldsymbol{\Psi}^\top \mathbf{B}_{\text{MS}} \boldsymbol{\Psi}}. \quad (62)$$

The regularized MS fit has not only the advantage that the curvature pull distribution is free of bias, another advantage is that the fit depends only on the MS scattering parameters, and no longer on the estimated MS errors (matrix \mathbf{D}_{MS}). Therefore, there is no need to estimate the MS angular error before (global) fitting. The downside is that the regularized fit introduces a bias for the fitted curvature as shown in Figure 5, which, however, becomes smaller if several triplets per track are combined. For regularized triplets, the curvature bias scales as:

$$\mathbb{E}[\kappa_{\text{MSreg}}] - \kappa^{\text{true}} = \frac{1}{n} \frac{\sigma_{\kappa_{\text{MSreg}}}^2}{\kappa^{\text{true}}} \quad (63)$$

with n being the number of triplets combined, and assuming that all triplets have the same curvature resolution¹⁰. A quantitative analysis of the biases is presented in Section 5.4.

For completeness, the formulas for the regularized local triplet are given in Appendix B.

5.4. Comparison of Regularized and Unregularized MS Fits

The curvature bias of the regularized and unregularized MS fit are quantitatively compared using an example: A relativistic particle with a momentum of 300 MeV/c is measured in a homogeneous magnetic field of 3 Tesla using

¹⁰The positive sign of the curvature bias is actually a requirement to cancel the negative MS normalization bias from Equation 57.

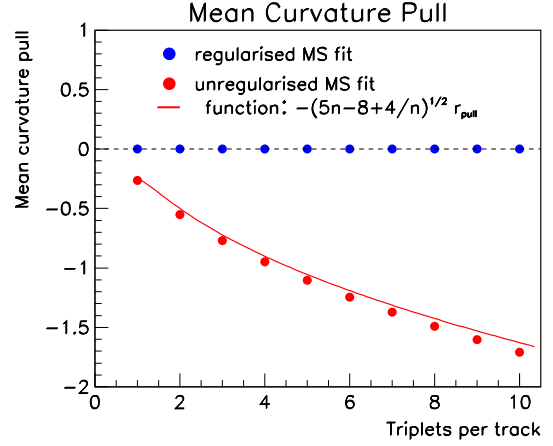


Figure 6: Simulated mean curvature pull (*circles*) as function of the number of triplets for a relative curvature (momentum) resolution of 23%. For more information, see also caption of Figure 5.

three tracking layers over a total distance of 60 mm. The material thickness of the middle tracking layer corresponds to 2% X_0 . The relative curvature (momentum) resolution of this setup is about 23%.

Assuming that hit position errors are negligible, the unregularized single triplet fit ($n = 1$) has no curvature bias whereas the regularized single triplet fit has a relative curvature bias of +5% (towards lower momenta), as shown in Figure 5. In contrast, the unregularized single triplet fit has a mean curvature pull of -25% (towards higher momenta) whereas the regularized single triplet fit has no pull, as shown in Figure 6.

Both plots also show the result for several (identical) triplets combined ($n > 1$). For the unregularized fit, the weighting bias causes an increasing shift towards negative curvatures (see Figure 5), which is quantitatively described by Equation 58. For the regularized fit, the curvature bias decreases inversely with the number of combined triplets according to Equation 63. Already in the case of two combined triplets, the (positive) curvature bias of the regularized MS fit is smaller than (negative) curvature bias of the unregularized fit. The negative mean curvature pull of the unregularized fit (see Figure 6) becomes even more negative if several triplets are combined, whereas the curvature pull of the regularized fit stays bias-free.

The negative curvature pull of the unregularized fit is a combined effect of the MS normalization bias (Section 5.1.1) and the weighting bias (Section 5.1.2). This combined bias can be described by a function that adds both sources quadratically:

$$\mathbb{E}[g_\kappa] = -\sqrt{\frac{8n^2 - 5n + 4}{n}} \frac{\sigma_{\kappa_{\text{MS}}}}{\kappa^{\text{true}}}. \quad (64)$$

As demonstrated for the discussed example, both the MS normalization bias and the weighting bias can significantly deteriorate the curvature measurement if the un-

regularized MS fit is used. Therefore, preference should be given to the regularized fit.

Finally, it should be mentioned that the fitting bias also occurs for other commonly used track fits. In both Kálmán filter and GBL, a prior is used to determine the MS angular errors, corresponding to the unregularized fit discussed above. To the author's knowledge, the regularized triplet-based MS fit is the only non-iterative method that guarantees a bias-free curvature (momentum) pull if the MS errors are dominant.

6. Calculation of Triplet Parameters

The triplet parameters are detector-specific and depend on the tracker geometry and the magnetic field. In this section, the four fundamental triplet parameters ($\tilde{\Phi}_0$, $\tilde{\Theta}_0$, ρ_Φ and ρ_Θ) are calculated for three typical and commonly used tracking detector designs: a homogeneous magnetic field, and spectrometer setup with a dipole field.

Moreover, track fits in regions without a magnetic field, as well as an algorithm for determining the triplet parameters in *any* magnetic field configuration, are discussed in the appendix (Appendix C and Appendix D).

6.1. Homogeneous Magnetic Field

The situation of a hit triplet in a homogeneous magnetic field is illustrated in Figure 7. The z -axis of the spherical coordinate system is aligned with the magnetic field direction, and the x - y plane is the bending plane. The line connecting hit 0 and 1 (hit 1 and 2) defines the azimuthal angle φ_{01} (φ_{12}) in the transverse plane and the polar angle ϑ_1 (ϑ_2) in the longitudinal s - z plane. Note that for a homogeneous magnetic field the polar angle of the particle is an invariant in free space.

The coordinate s is the arc length and describes the position on the trajectory in the transverse plane. The arc lengths of the two segments are denoted by s_{01} and s_{12} , and Φ_1 and Φ_2 are the corresponding bending angles. The kink angles in the bending and non-bending plane are given by:

$$\Delta\Phi = (\varphi_{12} - \varphi_{01}) - \frac{\Phi_1 + \Phi_2}{2}, \quad (65)$$

$$\Delta\Theta = \vartheta_2 - \vartheta_1. \quad (66)$$

The bending angles $\Phi_{1,2}$ and polar angles $\vartheta_{1,2}$ of the two segments have to fulfill the relations [8]:

$$\begin{aligned} \sin^2 \frac{\Phi_1}{2} &= \frac{1}{4} \kappa^2 d_{01}^2 + \kappa^2 z_{01}^2 \frac{\sin^2(\Phi_1/2)}{\Phi_1^2}, \\ \sin^2 \frac{\Phi_2}{2} &= \frac{1}{4} \kappa^2 d_{12}^2 + \kappa^2 z_{12}^2 \frac{\sin^2(\Phi_2/2)}{\Phi_2^2}, \end{aligned} \quad (67)$$

$$\begin{aligned} \sin \vartheta_1 &= \frac{1}{2} \kappa d_{01} \operatorname{cosec} \left(\frac{\kappa z_{01}}{2 \cos \vartheta_1} \right), \\ \sin \vartheta_2 &= \frac{1}{2} \kappa d_{12} \operatorname{cosec} \left(\frac{\kappa z_{12}}{2 \cos \vartheta_2} \right). \end{aligned} \quad (68)$$

These transcendental equations have multiple solutions. For most experiments, only the first solution is relevant¹¹, corresponding to $0 < |\Phi_i| \leq \pi$. In order to solve the equations above, the trajectory fulfilling the condition $\Delta\Phi = 0$ (no kink in the bending plane) is chosen as reference for the linearization, as motivated in Section 2.1. This reference trajectory corresponds to a circle solution in the bending plane, for which the transverse curvature, κ_\perp , is readily obtained from the three triplet hit positions, by means of:

$$\kappa_\perp = \frac{2 \sin(\varphi_{12} - \varphi_{01})}{d_{02}} \quad (69)$$

$$= 2 \frac{[(\vec{x}_1 - \vec{x}_0) \times (\vec{x}_2 - \vec{x}_1)]_z}{d_{01} d_{12} d_{02}}, \quad (70)$$

where transverse distance parameters, defined as $d_{kk'}^2 := (x_k - x_{k'})^2 + (y_k - y_{k'})^2$, enter. For the reference trajectory, the bending and polar angles are then given by:

$$\Phi_{1C} := 2 \arcsin \left(\frac{d_{01} \kappa_\perp}{2} \right), \quad (71)$$

$$\Phi_{2C} := 2 \arcsin \left(\frac{d_{12} \kappa_\perp}{2} \right), \quad (72)$$

$$\cos \vartheta_{1C} := \frac{z_{01}}{\sqrt{z_{01}^2 + d_{01}^2 \frac{\Phi_{1C}^2}{4 \sin^2 \Phi_{1C}/2}}}, \quad (73)$$

$$\cos \vartheta_{2C} := \frac{z_{12}}{\sqrt{z_{12}^2 + d_{12}^2 \frac{\Phi_{2C}^2}{4 \sin^2 \Phi_{2C}/2}}}, \quad (74)$$

where the index ‘‘C’’ indicates the circle solution.

From the first order linearization (Equation 8 and Equation 9), the four fundamental triplet parameters are eventually obtained:

$$\tilde{\Phi}_0 = \frac{1}{2} (\Phi_{1C} n_{1C} + \Phi_{2C} n_{2C}), \quad (75)$$

$$\begin{aligned} \tilde{\Theta}_0 &= \vartheta_{2C} - \vartheta_{1C} \\ &+ (1 - n_{2C}) \cot \vartheta_{2C} - (1 - n_{1C}) \cot \vartheta_{1C}, \end{aligned} \quad (76)$$

$$\rho_\Phi = -\frac{1}{2 \kappa_\perp} \left(\frac{\Phi_{1C} n_{1C}}{\sin \vartheta_{1C}} + \frac{\Phi_{2C} n_{2C}}{\sin \vartheta_{2C}} \right), \quad (77)$$

$$\rho_\Theta = (1 - n_{1C}) \frac{\cos \vartheta_{1C}}{\sin^2 \vartheta_{1C}} - (1 - n_{2C}) \frac{\cos \vartheta_{2C}}{\sin^2 \vartheta_{2C}}. \quad (78)$$

The fundamental triplet parameters are here given as function of two index parameters, which were first introduced in Ref.[8] and read¹²:

$$n_{1C} = \left(\frac{\Phi_{1C}}{2} \cot \frac{\Phi_{1C}}{2} \sin^2 \vartheta_{1C} + \cos^2 \vartheta_{1C} \right)^{-1} \quad (79)$$

$$n_{2C} = \left(\frac{\Phi_{2C}}{2} \cot \frac{\Phi_{2C}}{2} \sin^2 \vartheta_{2C} + \cos^2 \vartheta_{2C} \right)^{-1}. \quad (80)$$

¹¹An exception is the Mu3e experiment [9], where purposely also recurlers with $|\Phi_i| \geq \pi$ are measured.

¹²The index parameters were called α_1 and α_2 in [8].

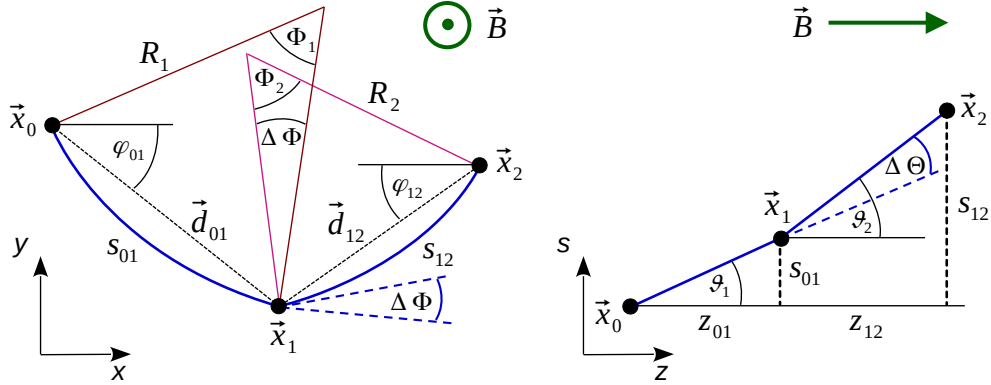


Figure 7: Sketch of a hit triplet in two projections: the x - y bending plane (left) and the s - z non-bending plane (right). Hit positions are given by the three points \vec{x}_0 , \vec{x}_1 and \vec{x}_2 . R_1 and R_2 are the transverse bending radii before and after the middle layer. s_{01} and s_{12} denote the transverse arc lengths and Φ_1 and Φ_2 the corresponding bending angles. d_{01} and d_{12} denote the transverse distance vectors between hits in the transverse plane and φ_{01} and φ_{12} are the corresponding azimuthal angles. $\Delta\Phi$ is the kink angle in the bending plane. In the non-bending plane, z_{01} and z_{12} define the longitudinal distances between adjacent hits, ϑ_1 and ϑ_2 the corresponding polar angles and $\Delta\Theta$ is the kink angle. Modified from Ref.[8].

Note that above index parameters might become singular for recurling tracks, i.e., $|\Phi_{1C,2C}| \geq \pi$. It should be remarked here that triplets, for which n_{1C} or n_{2C} are singular, can provide an excellent momentum resolution as MS uncertainties vanish in first order [8].

6.1.1. Small Bending Limit

In the limit of small bending angles, i.e., $\Phi_1 \rightarrow 0$ and $\Phi_2 \rightarrow 0$ (corresponding to high momentum tracks), or small polar angles, $\vartheta_1 \rightarrow 0$ and $\vartheta_2 \rightarrow 0$, the index parameters approach unity, $n_{1C} \rightarrow 1$ and $n_{2C} \rightarrow 1$. In this limit, the fundamental triplet parameters simplify to:

$$\lim_{\kappa \rightarrow 0} \tilde{\Phi}_0 = \varphi_{12} - \varphi_{01}, \quad (81)$$

$$\lim_{\kappa \rightarrow 0} \tilde{\Theta}_0 = \vartheta_2 - \vartheta_1, \quad (82)$$

$$\lim_{\kappa \rightarrow 0} |\rho_\Phi| = \frac{1}{2} \sqrt{d_{02}^2 + z_{02}^2}, \quad (83)$$

$$\lim_{\kappa \rightarrow 0} \rho_\Theta = 0. \quad (84)$$

In this limit, the parameters $\tilde{\Theta}_0$ and $\tilde{\Phi}_0$ become the triplet kink angles, the ρ_Φ parameter corresponds to the length of the line connecting the first and third triplet hit, and the ρ_Θ parameter vanishes. All fundamental triplet parameters are simple functions of the triplet geometry in this limit.

6.2. Spectrometer Setup with Dipole

Figure 8 shows the simplest spectrometer setup with three detector planes (triplet) and one dipole. The dipole has a thickness ν_B and is placed between detector layers 1 and 2 at distances ν_1 and ν_2 , respectively. In the following,

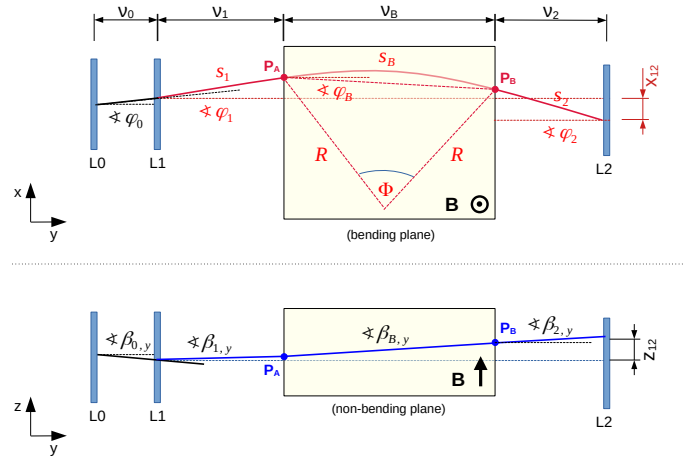


Figure 8: Sketch of a dipole spectrometer with three layers (L0-L2) with L1 being the scattering layer of the triplet. The upper half shows the $(x$ - y) bending plane and the definition of the azimuthal angles for the different track segments and the bending angle Φ ; the lower half shows the $(y$ - z) plane with the elevation angles β projected to the y -axis.

it is assumed that all measurement planes and the dipole entrance and exit windows are parallel. The magnetic field is pointing in z -direction such that the x - y plane is the bending plane.

For convenience, the elevation angle β is defined that measures the particle angle with respect to the x - y plane and is related to the polar angle via $\vartheta = \pi/2 - \beta$. Note that the elevation angle is an invariant in the plane transverse to the magnetic field, i.e., $\beta_1 = \beta_B = \beta_2$.

Since the region between tracking layers L0 and L1 has no magnetic field, it is trivial to calculate the angles φ_0 and β_0 for the first segment. For the trajectory between tracking layers L1 and L2, the situation is far more complicated: the trajectory has first a field-free segment, then the dipole segment and then another field-free segment.

First, the trajectory is calculated in the bending plane. The bending angle, Φ , is defined as ratio of the arc length, s_B , over the bending radius, R . Both parameters are also related to the dipole length ν_B , through:

$$\Phi = \frac{s_B}{R} = 2 \arcsin \frac{\nu_B}{2R \cos \varphi_B}, \quad (85)$$

with $\cos \varphi_B$ being the average azimuthal angle in the dipole field region¹³. The azimuthal angles in the field-free region are related to the bending angle in the dipole via:

$$\varphi_{1,2} = \varphi_B \mp \frac{\Phi}{2}. \quad (86)$$

With the above relation, the bending radius in Equation 85 is calculated as function of the azimuthal angle φ_1 :

$$R = \frac{\nu_B}{\sin(\varphi_1 + \Phi) - \sin \varphi_1}. \quad (87)$$

The horizontal offset, $x_{12} := x_2 - x_1$, measured between tracking layers L1 and L2, depends on all azimuthal angles and is given by:

$$\begin{aligned} x_{12} &= \nu_1 \tan \varphi_1 + \nu_B \tan \varphi_B + \nu_2 \tan \varphi_2 \\ &= \nu_1 \tan \varphi_1 + \nu_B \tan \left(\varphi_1 + \frac{\Phi}{2} \right) + \nu_2 \tan (\varphi_1 + \Phi). \end{aligned} \quad (88)$$

Since ν_1 , ν_2 and ν_3 are geometrical constants and x_{12} is measured, Equation 88 defines a unique relationship between the azimuthal angle φ_1 and the bending angle Φ . In lowest order, this equation is cubic in both φ_1 and $\Phi/2$, making it difficult to derive the solution for the general case (see also Section 6.2.1).

In the non-bending plane, the elevation angle, β_1 , is given through the relation:

$$\tan \beta_1 = \frac{z_{12}}{(s_1 + s_B + s_2)}, \quad (89)$$

with z_{12} being the measured vertical offset, $z_{12} := z_2 - z_1$. The parameters s_1 and s_2 are the lengths of the no-field track segments in the bending plane, given by:

$$s_1 = \nu_1 \sec \varphi_1, \quad (90)$$

$$s_2 = \nu_2 \sec(\varphi_1 + \Phi_{\varphi_1}). \quad (91)$$

Here the notation $\Phi_{\varphi_1} := \Phi(\varphi_1)$ is introduced, where the index indicates the functional dependence given by Equation 88.

Finally, using the bending radius (Equation 87) and the relation for the elevation angle (Equation 89) the 3D curvature is calculated as:

$$\begin{aligned} \kappa &= R^{-1} \cos \beta_1 = R^{-1} \sin \vartheta_1 \\ &= \frac{\sin(\varphi_1 + \Phi_{\varphi_1}) - \sin \varphi_1}{\nu_B} \times \\ &\quad \frac{1}{\sqrt{1 + \frac{z_{12}^2}{\left(\nu_1 \sin \varphi_1 + \nu_2 \sin(\varphi_1 + \Phi_{\varphi_1}) + \nu_B \frac{\Phi_{\varphi_1}}{\sin(\varphi_1 + \Phi_{\varphi_1}) - \sin \varphi_1} \right)^2}}}. \end{aligned} \quad (92)$$

This equation is non-linear in φ_1 and Φ_{φ_1} . Since the function $\Phi(\varphi_1)$ is also non-linear, the linearization around a reference solution is here much more complicated than in the case of a triplet in a homogeneous magnetic field.

As motivated in Section 2, the solution with zero kink angle in the bending plane is chosen as reference for the linearization; therefore we define:

$$\varphi_{1,\text{ref}} = \varphi_0. \quad (93)$$

In the following, the solution for the general case and the small bending approximation is discussed.

6.2.1. General Solution

The general solution involves solving Equation 88 numerically to determine the reference bending angle $\Phi_{\text{ref}} = \Phi(\varphi_{1,\text{ref}})$. With the help of Φ_{ref} , all parameters of the reference trajectory can be calculated; most importantly, the reference elevation angle, β_{ref} , using Equation 89 and the reference curvature, κ_{ref} , using Equation 92.

For the determination of the ρ parameters, the derivatives $d\kappa/d\varphi_1$ and $d\kappa/d\vartheta_1$ are needed. An analytical solution can be derived by differentiation of Equation 92 and Equation 89, respectively, and by using the relations:

$$\rho_{\Theta} = \rho_{\Phi} \frac{d(\Delta\Theta)}{d(\Delta\Phi)} = \rho_{\Phi} \frac{d\vartheta_1}{d\varphi_1} = -\rho_{\Phi} \frac{d\beta_1}{d\varphi_1}. \quad (94)$$

However, the equations obtained in this way will be very unwieldy. In fact, it is much easier to determine the ρ parameters numerically from a small variation, ϵ , of the azimuthal angle $\varphi_{1,\text{ref}} \rightarrow \varphi'_{1,\text{ref}} = \varphi_{1,\text{ref}} + \epsilon$. This yields a second solution, which is denoted as κ'_{ref} and $\beta'_{1,\text{ref}}$. The fundamental triplet parameters are then given by:

$$\rho_{\Theta} = -\frac{\beta'_{1,\text{ref}} - \beta_{1,\text{ref}}}{\kappa'_{\text{ref}} - \kappa_{\text{ref}}}, \quad (95)$$

$$\rho_{\Phi} = \frac{\epsilon}{\kappa'_{\text{ref}} - \kappa_{\text{ref}}}, \quad (96)$$

$$\tilde{\Theta}_0 = -\rho_{\Theta} \kappa_{\text{ref}} - (\beta_{1,\text{ref}} - \beta_0), \quad (97)$$

$$\tilde{\Phi}_0 = -\rho_{\Phi} \kappa_{\text{ref}}. \quad (98)$$

6.2.2. Approximation for Small Bending Angles

In the case of small bending angles Φ , Equation 88 can be linearized to first order in Φ . In this approximation,

¹³In this calculation, stray fields are neglected.

the fundamental triplet parameters are given by:

$$\tilde{\Phi}_0 \approx \arctan\left(\frac{x_{12}}{y_{12}}\right) - \varphi_0, \quad (99)$$

$$\tilde{\Theta}_0 \approx \arctan\left(\frac{z_{12}}{d_{12}}\right) - \vartheta_0, \quad (100)$$

$$\rho_\Phi \approx \frac{\sqrt{d_{12}^2 + z_{12}^2}}{2} \frac{\nu_B}{y_{12}} \left(1 - \frac{\nu_2 - \nu_1}{y_{12}}\right), \quad (101)$$

$$\rho_\Theta \approx 0, \quad (102)$$

with $d_{12} := \sqrt{x_{12}^2 + y_{12}^2}$ being the distance between hit 1 and 2 in the bending plane. Similar to the weak bending case in a homogeneous magnetic field, the parameter ρ_Θ vanishes here. For symmetric setups, i.e., $\nu_1 = \nu_2$, the parameter ρ_Φ is equivalent to half the effective track length in the dipole field. In the limit $\nu_1 \rightarrow 0$ and $\nu_2 \rightarrow 0$ (the tracking layer L1 and L2 are positioned at the dipole entrances and exit), this parameter becomes: $\rho_\Phi = \sqrt{d_{12}^2 + z_{12}^2}/2$. Similar to the homogeneous magnetic field setup, the ρ_Φ parameter corresponds to half the length that the particle travels in the magnetic field, consistent with the naive expectation from the Lorentz force law.

7. Energy Loss Correction

In addition to MS, detector material causes energy loss through ionization, and in case of electrons and positrons also Bremsstrahlung. The expected energy loss depends on the effective path length in the material, which is the same used for the calculation of the MS parameters and already known at triplet level.

The following sections describe a simple energy loss correction procedure based on the expected energy loss for the local (Section 7.1) and global track fit (Section 7.2). This correction is well suited for thin tracking layers. For thick tracking layers, however, energy straggling might be significant, requiring a combined fit of the track parameters and the energy losses, which is presented in Section 7.3.

For sake of simplicity, it is assumed that the particle is highly relativistic, such that the relation $p \sim E$ can be exploited. Furthermore, the calculations are performed for a homogeneous magnetic field.

7.1. Energy Loss Correction in Local Fit

Energy loss at the middle tracking layer of a triplet changes the 3D curvature, thus altering the trajectory and the triplet parameters, as shown in Figure 9. Under the assumption of small energy losses, Δ_E , the curvature change is given by:

$$\Delta\kappa = \kappa_{2S} - \kappa_{1S} = \frac{\Delta_E}{E} \kappa_{1S} \approx \frac{\Delta_E}{qB} \kappa_{1S}^2, \quad (103)$$

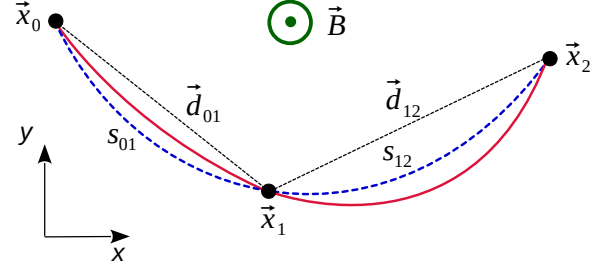


Figure 9: Sketch showing in a homogeneous magnetic field a trajectory with energy loss at the middle triplet layer (red solid line). For comparison a trajectory without energy loss is shown, which also connects all hits (blue dashed line).

with κ_{1S} and κ_{2S} being the curvature of the first and second segment, respectively. The curvatures before and after the energy loss are related to the solution of the standard fit without energy loss, κ , through

$$\kappa_{1S} = \kappa - \frac{s_{12}}{s_{02}} \Delta\kappa, \quad (104)$$

$$\kappa_{2S} = \kappa + \frac{s_{01}}{s_{02}} \Delta\kappa. \quad (105)$$

Due to the curvature difference between the two segments, the azimuthal angles are rotated with respect to the $\Delta_E = 0$ solution. Using the notation from Section 2.1, the azimuthal angles at the three hit positions are given by:

$$\Delta\phi_{01} = \phi_{01}^{\Delta_E} - \phi_{01} = + \frac{s_{01}s_{12}}{2s_{02}} \Delta\kappa \sin \hat{\vartheta}, \quad (106)$$

$$\Delta\phi_{10} = \phi_{10}^{\Delta_E} - \phi_{10} = - \frac{s_{01}s_{12}}{2s_{02}} \Delta\kappa \sin \hat{\vartheta}, \quad (107)$$

$$\Delta\phi_{12} = \phi_{12}^{\Delta_E} - \phi_{12} = - \frac{s_{01}s_{12}}{2s_{02}} \Delta\kappa \sin \hat{\vartheta}, \quad (108)$$

$$\Delta\phi_{21} = \phi_{21}^{\Delta_E} - \phi_{21} = + \frac{s_{01}s_{12}}{2s_{02}} \Delta\kappa \sin \hat{\vartheta}. \quad (109)$$

Note that the angles ϕ_{10} and ϕ_{12} change by the same rotation angle; thus the kink angles and the fit quality of the local fit are not affected by the energy loss, in first order.

7.2. Energy Loss Correction in Global Fit

The relation between different segment curvatures is given by summing up the curvature changes:

$$\kappa_{1S,j} (= \kappa_{2S,j}) = \kappa_{1S,0} + \sum_{j'=0}^{j-1} \Delta\kappa_{j'}, \quad (110)$$

where $\Delta\kappa_{j'}$ denotes the curvature change due to energy loss at the middle layer of triplet j' and $\kappa_{1S,0}$ is the curvature of the first segment of the track. By defining the integrated energy loss for triplet j :

$$I_j := \sum_{j'=0}^j \Delta_{E_{j'}},$$

Equation 110 can be rewritten as:

$$\begin{aligned}\kappa_{1S,j} &= \kappa_{1S,0} + \frac{I_{j-1}}{qB} \kappa_{1S,0}^2 \\ &\approx \kappa_{1S,0} \left(1 + \frac{2I_{j-1}}{qB} \hat{\kappa}_j \right) - \frac{I_{j-1}}{qB} \hat{\kappa}_j^2\end{aligned}\quad (111)$$

where $\hat{\kappa}_j$ denotes the curvature measurement from the local fit of triplet j . The segment curvature, $\kappa_{1S,j}$, depends quadratically on the initial track curvature, $\kappa_{1S,0}$, is linearized in the second line of Equation 111, in order to avoid higher order terms in the global fit. This linearization is possible as the energy loss in tracking detectors is typically small compared to the particle energy¹⁴.

By using Equation 104, the average triplet curvature κ_j , can be related to the initial track curvature via:

$$\begin{aligned}\kappa_j &\approx \kappa_{1S,0} \left(1 + \frac{2I_j^*}{qB} \hat{\kappa}_j \right) - \frac{I_j^*}{qB} \hat{\kappa}_j^2, \\ \text{with } I_j^* &= I_{j-1} + \frac{s_{12}}{s_{02}} \Delta_{E,j}.\end{aligned}\quad (112)$$

By comparing Equation 112 with the linearization ansatz in Equation 16 and Equation 17, one sees that the energy loss in the triplet corresponds to a re-interpretation of the triplet parameters. The linear relation between κ_j and $\kappa_{1S,0}$ allows the use of the global track fit formulas from Section 3 by making the following substitutions:

$$\tilde{\Theta}_j \rightarrow \tilde{\Theta}'_j = \tilde{\Theta}_j - \rho_{\Theta,j} \frac{I_j^*}{qB} \hat{\kappa}_j^2, \quad (113)$$

$$\tilde{\Phi}_j \rightarrow \tilde{\Phi}'_j = \tilde{\Phi}_j - \rho_{\Phi,j} \frac{I_j^*}{qB} \hat{\kappa}_j^2, \quad (114)$$

$$\rho_{\Theta,j} \rightarrow \rho'_{\Theta,j} = \rho_{\Theta,j} \left(1 + \frac{2I_j^*}{qB} \hat{\kappa}_j \right), \quad (115)$$

$$\rho_{\Phi,j} \rightarrow \rho'_{\Phi,j} = \rho_{\Phi,j} \left(1 + \frac{2I_j^*}{qB} \hat{\kappa}_j \right). \quad (116)$$

With above re-interpretation of the fundamental triplet parameters, the expected energy loss can easily be included in the triplet track fit¹⁵.

7.3. Combined Track and Energy Loss Fit

For thick tracking detectors, energy straggling might be significant, motivating to include the energy losses in the tracking layers as additional fit parameters. Energy losses have usually non-Gaussian tails. However, for the sake of simplicity, a normal distribution is used to derive

¹⁴This approach is not valid in case of catastrophic Bremsstrahlung of electrons and positrons.

¹⁵It is important to note that the locally fitted curvatures $\hat{\kappa}_j$ should only be used in above equations if they are reliably measured by the triplets. Otherwise, a better strategy is to repeat the fit, after neglecting the energy loss in the first step, and using the curvature result of the first fit as reference.

the fit formulas. A difficulty arises from the quadratic curvature dependence of the curvature shifts (see e.g. Equation 103) that creates non-linearities in the fit¹⁶. This problem can be tackled either by using the linearization ansatz from the previous section (Equation 113 to 116) or by re-iterating the fit. In order not to add too much complexity to the discussion, it is assumed that the track curvature (momentum) is known well enough, either from the local triplets or a previous global fit, such that the curvature shifts can be approximated by:

$$\kappa_j - \kappa_{1S,0} \approx \frac{I_j^*}{qB} \kappa_{\text{pre}}^2, \quad (117)$$

with κ_{pre} being the curvature obtained pre-fit.

If hit position errors are neglected, the fit function in matrix representation reads:

$$\begin{aligned}\chi^2(\kappa_{1S,0}, \boldsymbol{\delta}_E) &= \boldsymbol{\delta}_E^\top \mathbf{D}_{\text{loss}} \boldsymbol{\delta}_E + \\ &(\boldsymbol{\Psi} + \boldsymbol{\rho} \kappa_{1S,0} - \mathbf{R} \boldsymbol{\Delta}_E)^\top \mathbf{D}_{\text{MS}} (\boldsymbol{\Psi} + \boldsymbol{\rho} \kappa_{1S,0} - \mathbf{R} \boldsymbol{\Delta}_E),\end{aligned}\quad (118)$$

with $\kappa_{1S,0}$ being the fit parameter describing the curvature of the first track segment, $\boldsymbol{\Delta}_e$ being a vector describing the energy losses for each tracking layer, $\boldsymbol{\delta}_E$ being a vector (fit variable) describing the difference between the fitted energy losses and the expected energy losses, according to $\boldsymbol{\delta}_E := \boldsymbol{\Delta}_E - \boldsymbol{\Delta}_E^{\text{exp}}$, and \mathbf{D}_{loss} being the energy loss precision matrix (inverse covariance matrix).

The relation between the energy losses and kink angle changes is described by the matrix \mathbf{R} , which is of size $2 n_{\text{triplet}} \times n_{\text{triplet}}$ and given by:

$$\mathbf{R} = \frac{\kappa_{\text{pre}}^2}{qB} \begin{pmatrix} \boldsymbol{\rho}_\Theta \circ \boldsymbol{\Sigma} \\ \boldsymbol{\rho}_\Phi \circ \boldsymbol{\Sigma} \end{pmatrix}. \quad (119)$$

The operator \circ is the element-wise Schur product, and $\boldsymbol{\Sigma}$ is a quadratic *integration matrix*, which sums up all energy losses before the respective tracking layer:

$$(\boldsymbol{\Sigma})_{jj'} = \begin{cases} 1 & \text{if } j > j' \\ \left(\frac{s_{12}}{s_{02}} \right)_j & \text{if } j = j' \\ 0 & \text{if } j < j' \end{cases}.$$

Note that the index j runs over all triplets and that the energy loss in the very first tracking layer ($k = 0$) and the last tracking layer ($k = n_{\text{hit}} - 1$) are not accounted for in the fit.

The minimization of Equation 118 gives the result:

$$\kappa_{\text{loss}} = - \frac{\boldsymbol{\rho}^\top \mathbf{K}_{\text{loss}} \boldsymbol{\Psi}_{\text{loss}}}{\boldsymbol{\rho}^\top \mathbf{K}_{\text{loss}} \boldsymbol{\rho}}, \quad (120)$$

$$\sigma_{\kappa_{\text{loss}}}^2 = \frac{1}{\boldsymbol{\rho}^\top \mathbf{K}_{\text{loss}} \boldsymbol{\rho}}, \quad (121)$$

¹⁶This problem does not arise if the 3D radius $R_{3D} = \kappa$ is chosen as fit parameter, as it is done in Ref.[8].

with \mathbf{K}_{loss} being the triplet precision matrix for the energy loss fit, defined as:

$$\mathbf{K}_{\text{loss}}^{-1} = \mathbf{D}_{\text{MS}}^{-1} + \mathbf{R} \mathbf{D}_{\text{loss}}^{-1} \mathbf{R}^\top, \quad (122)$$

and Ψ_{loss} being a modified kink angle vector, which includes effective kinks from the energy loss:

$$\Psi_{\text{loss}} = \Psi + \mathbf{R} \Delta_E^{\text{exp}}. \quad (123)$$

The fit quality then becomes:

$$\chi_{\text{loss}}^2 = \Psi_{\text{loss}}^\top \mathbf{K}_{\rho_{\text{loss}}} \Psi_{\text{loss}}, \quad (124)$$

with

$$\mathbf{K}_{\rho_{\text{loss}}} = \left(\mathbf{K}_{\text{loss}} - \frac{\mathbf{K}_{\text{loss}} \rho \rho^\top \mathbf{K}_{\text{loss}}}{\rho^\top \mathbf{K}_{\text{loss}} \rho} \right). \quad (125)$$

Above results have exactly the same form as the general fit that takes into account hit position errors, except that the hit residuals are replaced by the energy losses and the matrix $\vec{\mathbf{H}}$ is replaced by the matrix \mathbf{R} . Accordingly, one obtains for the fitted energy loss vector:

$$\Delta_E = \Delta_E^{\text{exp}} + \mathbf{D}_{\text{loss}}^{-1} \mathbf{R}^\top \mathbf{K}_{\rho_{\text{loss}}} \Psi_{\text{loss}}, \quad (126)$$

and for the corresponding covariance matrix:

$$\text{Cov}_{\delta_E} = \mathbf{D}_{\text{loss}}^{-1} - \mathbf{D}_{\text{loss}}^{-1} \mathbf{R}^\top \mathbf{K}_{\rho_{\text{loss}}} \mathbf{R} \mathbf{D}_{\text{loss}}^{-1}. \quad (127)$$

It is straightforward to also include hit errors in the fit.

8. Triplet Fit Parallelization and Computational Effort

The GTTF consists of three main steps: the calculation of the triplet parameters, the local triplet fit (as optional filtering step), and the global triplet track fit. The savings potential through parallel computing is discussed for each step.

Triplet Parameters and Hit Gradients. Two main cases can be distinguished. In the most general case (e.g. inhomogeneous magnetic field) the triplet parameters need to be derived from at least 2×4 track extrapolations per triplet (see Appendix D). These track extrapolations are *independent* and can be fully parallelized.

In case that an analytical solution for the triplet parameters exists (e.g. homogeneous magnetic field, see Section 6.1), no computationally expensive track extrapolations are required. The determination of the up to 3×3 hit gradients only involves simple geometrical (re-)calculations, which are fully parallelizable. If MS errors dominate, the calculation of the hit gradients is not required.

Since the triplet parameters of all triplets are independent, the calculation of the triplet parameters can be fully parallelized. This step can significantly profit from parallel hardware architectures like GPUs.

Local Triplet Fit as Filtering Step. Hit triplets are often used as seeds in track reconstruction; an early filtering step can be very useful to reduce hit combinatorics and speed up processing time. The filtering step consists of calculating the local triplet fit quality (Equation 47) and applying a quality cut. Only for accepted triplets, the momentum and its error should be calculated to enable checking the consistency of the momentum with other triplets. Also this step can be fully parallelized.

Global Triplet Track Fit. In the general case, where hit position errors cannot be neglected, the inversion of the precision matrix \mathbf{K}^{-1} is the most time-consuming step. The limited ability to accelerate this step highlights the importance of the local triplet fit as an early filtering step.

The situation is different in case of dominant MS errors where the precision matrix \mathbf{K}^{-1} is diagonal. The global fit quality, the track curvature, and its error can then be easily calculated from simple sums, according to Equation 31 to 33. The computational effort is marginal and the required calculations can be efficiently implemented on parallel hardware architectures like GPUs.

9. Tracking Regimes

In this work, a mathematical concept for track fitting based on the triplet representation has been developed. This concept can also be used for track resolution studies, which aim to optimize the track parameter resolution, for example in the context of designing new tracking detectors. Depending on the source and also the size of the dominant tracking errors, different *tracking regimes* can be defined based on two quantities, namely the *tracking scale parameter* and the *curvature significance parameter*.

9.1. The Tracking Scale Parameter

The relevant quantities that enter the triplet precision matrix are $\Gamma_{\Phi\Phi}^*$ and $\Gamma_{\Theta\Theta}^*$, which combine the hit position and MS errors (see Section 4). The relative fraction of hit position errors (variance) is used to define two tracking scale parameters:

$$\mu_{\Phi}^2 := \frac{\Gamma_{\Phi\Phi}}{\Gamma_{\Phi\Phi}^*}, \quad \mu_{\Theta}^2 := \frac{\Gamma_{\Theta\Theta}}{\Gamma_{\Theta\Theta}^*}. \quad (128)$$

The values of μ_{Φ} and μ_{Θ} are in the range from 0 for dominant MS errors (low momentum) to 1 for dominant hit position errors (high momentum).

The tracking scale parameters are of practical relevance for track fitting. In the case that the scale parameters are small ($\mu_{\Phi, \Theta} \lesssim 0.15$), the fast MS fit can be used¹⁷, whereas in all other cases the general fit should be used, which requires the inversion of the precision matrix \mathbf{K}^{-1} (Equation 26). The tracking scale parameter is therefore an indicator for how fast the track fit can be performed.

¹⁷For $\rho_{\Phi}^2 \gg \rho_{\Theta}^2$ (small bending), only the tracking scale parameter μ_{Φ} is relevant.

9.2. The Curvature Significance Parameter

The curvature significance parameter, ξ , is defined by the ratio of the curvature over its error:

$$\xi^2 := \frac{\kappa^2}{\sigma_\kappa^2}, \quad (129)$$

and quantifies how precisely the track curvature is measured. The parameter allows to distinguish between the strong bending regime, $\xi^2 \gg 1$, where a momentum measurement is possible, and the weak bending regime, $\xi^2 \approx 0$, where no momentum measurement is possible.

9.2.1. Dominant MS Uncertainties ($\mu^2 = 0$)

For a tracking detector in a homogeneous magnetic field, where the relation $\rho_\Phi^2 \gg \rho_\Theta^2$ holds, one obtains the following relation for dominant MS uncertainties:

$$\xi_{\text{MS}}^2 = \frac{\kappa_{\text{MS}}^2}{\sigma_{\kappa_{\text{MS}}}^2} \approx \frac{\tilde{\Phi}_0^2}{\sigma_{\tilde{\Phi}_0}^2} \approx \frac{a_{02}^2}{4b_{\text{MS}}^2} \quad (130)$$

where for the second approximation the relations $\Delta\Phi \approx 2\tilde{\Phi}_0 \approx a_{02} \kappa$ (Equation 83) and $\sigma_{\text{MS}} = |\kappa| b_{\text{MS}}$ (Equation 3) are used. This parameter is essentially given by the ratio of the total triplet length, a_{02} , over the scattering parameter, b_{MS} , and does not depend on the particle momentum. ξ_{MS} therefore characterizes the tracking detector quality if MS is dominant. The requirement to measure the track curvature with 3σ significance corresponds to the condition $\frac{a_{02}}{2b_{\text{MS}}} \gtrsim 3$, a criterion first formulated in Ref.[8].

It should be remarked that ξ_{MS} is related to the curvature bias discussed in Section 5 and that that for $\xi_{\text{MS}} < 10$ significant curvature biases ($> 1\%$) can occur.

9.2.2. General case

For non-negligible hit position errors (general case), the curvature significance parameter can be easily derived from Equation 130 using the tracking scale parameter:

$$\xi = \xi_{\text{MS}} \cdot \sqrt{1 - \mu_\Phi^2}, \quad (131)$$

again assuming that $\rho_\Phi^2 \gg \rho_\Theta^2$. As expected, the curvature significance degrades with increasing hit position errors. Since the tracking scale parameter is momentum dependent, the generalized curvature significance also becomes momentum dependent.

9.3. Tracking Regimes of Example Pixel Detectors

In Figure 10 the $\mu_\Phi - 1/\xi_{\text{scatt}}$ parameter space is shown for several pixel detectors: the ALICE experiment [15, 16], the ATLAS experiment [17], and the Mu3e experiment [9]. These detectors have been selected here, as they cover a very wide range of particle momenta from $\mathcal{O}(10 \text{ MeV}/c)$ at the Mu3e experiment up to $\mathcal{O}(1000 \text{ GeV}/c)$ at the ATLAS experiment. For all detectors the tracking regime parameters are derived from hit triplets in the central region of the detector.

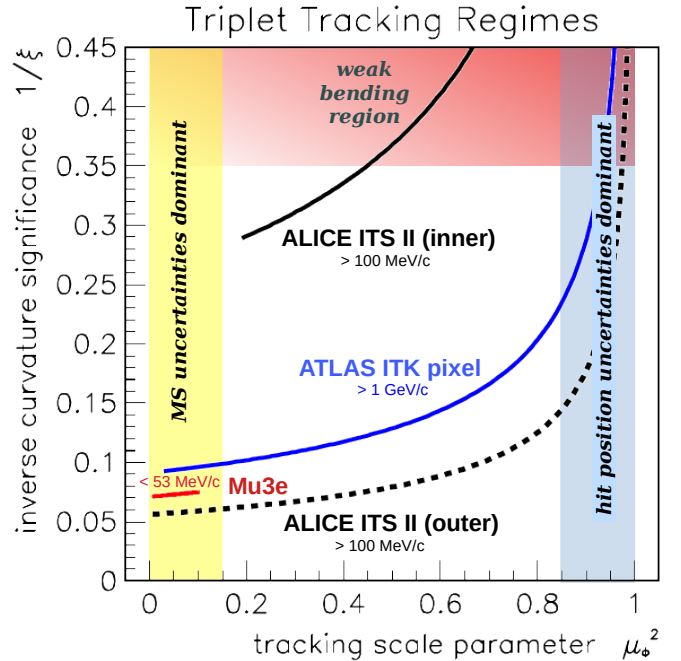


Figure 10: Parameter space spanned by the normalized MS parameter scale ξ_{scatter} and the tracking scale parameter μ_Φ for various pixel tracking detectors: ALICE ITS II inner and outer pixel tracking detector (black), ATLAS ITK (blue) and Mu3e (red). The horizontal lines cover the momentum range 0.1 – 100 GeV/c for ALICE, 1 – 1000 GeV/c for ATLAS, and 10 – 53 MeV/c for Mu3e.

The pixel tracker comparison starts with the ITS II detector [15, 16] of the ALICE experiment that is in operation since 2024. It consists of three inner pixel layers with a radiation length of $X/X_0 = 0.35\%$ and four outer pixel layers with an radiation length of $X/X_0 = 1\%$. The distance between the inner pixel layers is only $\sim 10 \text{ mm}$, which, together with the relatively moderate field of $B = 0.5 \text{ T}$, results in a low curvature significance of $\xi_{\text{MS}} \sim 3.8$, despite the small amount of tracking material. With the inner ITS II detector, a 3σ measurement of track curvatures is therefore only possible at low momenta below $p \lesssim 150 \text{ MeV}/c$. However, it should be mentioned that the main purpose of the inner ITS II detector is vertexing and not the momentum measurement.

The situation is different for the outer ITS II detector, where the tracking layers are separated by about 80 mm. The curvature significance for low-momentum tracks is $\xi_{\text{MS}} \sim 18$ and a 3σ measurement of track curvatures is possible for a single triplet up to 15 GeV/c, thanks to the high resolution of the ALPIDE sensors [18].

The ITK tracking system[17] of the high luminosity upgraded ATLAS experiment was optimized to reconstruct charged particles at very high particle rates with up to 200 collisions per cross section. Similar to the inner ITS II detector, the main purpose of the ATLAS pixel detector is to reconstruct primary and secondary vertices. Due to the higher radiation length per tracking layer of about $X/X_0 = 1.5\%$, the curvature significance is only $\xi_{\text{MS}} \sim 11$ for low-momentum tracks. A 3σ measurement of the

curvature is possible for a single triplet up to $20 \text{ GeV}/c$, thanks to the high field of $B = 2 \text{ T}$.

The Mu3e pixel detector [9] has an ultra-light pixel detector design with a radiation length of about $X/X_0 = 0.11 \%$ per tracking layer, and was optimized for tracking low-momentum electrons and positrons from muon decays in the momentum range $12 - 53 \text{ MeV}/c$. The tracking scale parameter is very small $\mu_\Phi^2 \leq 0.1$ for all momenta, such that the fast MS track fit can be exploited for all tracks. The curvature significance is about $\xi \sim 14$ in the full momentum range.

To summarize, both the tracking scale parameter μ_Φ and the curvature significance ξ give important information about the tracking regime and can help to optimize the fitting strategy. Another example is track reconstruction: triplets with high curvature significance ξ restrict the momentum space much more than low ξ triplets, making them much better suited for track extrapolations and momentum consistency checks with other triplets.

10. Summary

In this work, a new triplet-based track fit was presented, which is generic and takes into account material effects such as MS and energy loss, as well as measurement uncertainties. The track fit formulas are independent of the magnetic field configuration. This is accomplished by utilizing a universal representation of triplet parameters as input. The triplet parameters contain all relevant information about the triplet geometry, the material effects and the magnetic field.

It was shown that the triplet representation leads to simple formulas for the fitted track parameters and the fit quality, and that the results can be written in analytical closed-form as a function of the triplet parameters. This makes the triplet-based track fit universal, since the same track fitting code can be used for all tracking detectors, regardless of detector-specific geometry and field configuration. Only the calculation of the triplet parameters is detector-specific.

For practical applications, the triplet parameters have been calculated for different tracking detector setups: for a homogeneous magnetic field, for a spectrometer setup with an ideal dipole, and for triplets in zero magnetic field. It was shown that in the case of small track bending (high momentum region), the fundamental triplet parameters are very simple geometrical quantities. In addition, an algorithm employing track extrapolation was presented that enables the calculation of the triplet parameters for inhomogeneous magnetic fields.

The fit of a triplet trajectory is over-constrained by one degree of freedom. For track finding, this allows for filtering of triplets at an early stage of track reconstruction. The optional filtering step, therefore, offers a big potential to accelerate computing time. Furthermore, since all triplets are independent, the triplet-based track fit can be

completely parallelized, with the exception of one matrix inversion, which is required in the global track fit if hit position errors can not be neglected. Due to the high degree of parallelization, the GTTF is ideal for the implementation on parallel hardware architectures such as GPUs.

In this work, all relevant equations are provided to fully describe the fitted trajectory from the first to the last hit of a trajectory. For track extrapolation and propagation of errors, we refer to the literature [19].

The output of the GTTF is the particle momentum (curvature) at the start of the trajectory and the residuals including the full hit covariance matrix. Similar to the GBL [4, 5], the GTTF is well suited for track-based alignment SW packages like Millepede II [6, 7]. In contrast to the GBL, the triplet fit is unseeded, i.e., no approximate solution is required as input to the fit.

Furthermore, fitting biases of the track fit were discussed. These biases are a consequence of the momentum dependence of MS process; they are shown to be unavoidable in track fits if MS errors dominate and the particle momentum is not known a priori. Mitigation strategies have been discussed and a regularized track fit was presented, which significantly reduces this bias.

Last but not least, the triplet concept extends beyond track fitting; it can also be used to compute so-called tracking scale parameters to characterize different tracking regimes. Dividing the phase space into tracking regimes is very useful for track fit optimization and also for tracking detector design studies.

The optimization (acceleration) of track fits is of great importance for track reconstruction in real-time applications at high particle rates, e.g. at hadron colliders. Since most particles produced in hadron interactions have low momenta, computational time for track fits can be saved by always using the fast MS triplet fit first, which is also the correct tracking model if MS uncertainties are dominant. The general fit, which necessitates matrix inversion, should only be employed if the MS-fit fails and a recovery of the fit quality is possible if hit position errors are included. However, a discussion of the optimal implementation of the GTTF for experiment-specific applications is beyond the scope of this work.

Acknowledgments

The author thanks Niklaus Berger, Sebastian Dittmeier, Alexandr Kozlinskiy, and Christof Sauer for many useful discussions on this topic and for proofreading.

A. Global Fit for Dominant Hit Position Errors

In the limit of dominant hit position uncertainties, the MS errors can be neglected. According to Equation 26, the precision matrix becomes:

$$\mathbf{K} \rightarrow \mathbf{K}_{\text{hit}} := (\vec{\mathbf{H}} \vec{\mathbf{D}}_{\text{hit}}^{-1} \vec{\mathbf{H}}^{\top})^{-1}. \quad (\text{A.1})$$

The 3D curvature and its uncertainties are then given by:

$$\kappa_{\text{hit}} = \frac{\boldsymbol{\rho}^\top \mathbf{K}_{\text{hit}} \boldsymbol{\Psi}}{\boldsymbol{\rho}^\top \mathbf{K}_{\text{hit}} \boldsymbol{\rho}}, \quad (\text{A.2})$$

$$\sigma_{\kappa_{\text{hit}}}^2 = \frac{1}{\boldsymbol{\rho}^\top \mathbf{K}_{\text{hit}} \boldsymbol{\rho}}. \quad (\text{A.3})$$

Furthermore, the hit positions shifts and the corresponding covariance matrix are given by:

$$\vec{\delta}_{\text{hit}} = \vec{\mathbf{D}}_{\text{hit}}^{-1} \vec{\mathbf{H}}^\top \mathbf{K}_{\rho_{\text{hit}}} \boldsymbol{\Psi}, \quad (\text{A.4})$$

$$\mathbf{Cov}_{\delta_{\text{hit}}} = \vec{\mathbf{D}}_{\text{hit}}^{-1} - \vec{\mathbf{D}}_{\text{hit}}^{-1} \vec{\mathbf{H}}^\top \mathbf{K}_{\rho_{\text{hit}}} \vec{\mathbf{H}} \vec{\mathbf{D}}_{\text{hit}}^{-1}. \quad (\text{A.5})$$

Here, $\mathbf{K}_{\rho_{\text{hit}}}$ is defined similar to Equation 28:

$$\mathbf{K}_{\rho_{\text{hit}}} = \left(\mathbf{K}_{\text{hit}} - \frac{\mathbf{K}_{\text{hit}} \boldsymbol{\rho} \boldsymbol{\rho}^\top \mathbf{K}_{\text{hit}}}{\boldsymbol{\rho}^\top \mathbf{K}_{\text{hit}} \boldsymbol{\rho}} \right).$$

Finally, the fit quality is given by:

$$\chi_{\text{hit}}^2 = \boldsymbol{\delta}^\top \vec{\mathbf{D}}_{\text{hit}} \boldsymbol{\delta} \quad (\text{A.6})$$

$$= \boldsymbol{\Psi}^\top \mathbf{K}_{\rho_{\text{hit}}} \boldsymbol{\Psi}. \quad (\text{A.7})$$

Note that in the first line of Equation A.6 the sums are executed over all hit uncertainty directions whereas in the second line (Equation A.7) the sums run over twice the number of triplets.

B. Regularized Local MS Fit

The formulas for the regularized global MS fit are discussed in Section 5.3. For a single triplet, the fit result is given by:

$$\kappa_{\text{MSreg}} = - \frac{\tilde{\Phi}_0^2 \sin^2 \hat{\vartheta} + \tilde{\Theta}_0^2}{\rho_\Phi \tilde{\Phi}_0 \sin^2 \hat{\vartheta} + \rho_\Theta \tilde{\Theta}_0}, \quad (\text{B.1})$$

$$\sigma_{\kappa_{\text{MSreg}}} = b_{\text{MS}} \frac{(\tilde{\Phi}_0^2 \sin^2 \hat{\vartheta} + \tilde{\Theta}_0^2)^{\frac{3}{2}}}{(\tilde{\Phi}_0 \rho_\Phi \sin^2 \hat{\vartheta} + \tilde{\Theta}_0 \rho_\Theta)^2}, \quad (\text{B.2})$$

$$\chi_{\text{MSreg}}^2 = \frac{1}{b_{\text{MS}}^2} \frac{(\tilde{\Phi}_0 \rho_\Theta - \tilde{\Theta}_0 \rho_\Phi)^2}{\tilde{\Phi}_0^2 + \tilde{\Theta}_0^2 / \sin^2 \hat{\vartheta}}. \quad (\text{B.3})$$

C. Triplet in Zero Magnetic Field

In the case of zero magnetic field, the triplet trajectory is described by two straight lines with a kink. Although the momentum cannot be measured directly using the Lorentz force (the triplet ρ -parameters are zero), the amount of MS at the middle tracking layer is an indirect measure of the momentum. The compatibility of the kink angles with MS theory can be tested using:

$$\chi_{\text{MS},B=0}^2 = \boldsymbol{\Psi}^\top \mathbf{D}_{\text{MS}}(p) \boldsymbol{\Psi}, \quad (\text{C.1})$$

where hit position errors are neglected for sake of simplicity. Because of the momentum dependence of the MS errors: $\sigma_{\text{MS}} \propto 1/p$, Equation C.1 can be rescaled:

$$\chi_{\text{MS},B=0}^2 = \frac{p^2}{p_0^2} (\boldsymbol{\Psi}^\top \mathbf{D}_{\text{MS}}(p_0) \boldsymbol{\Psi}), \quad (\text{C.2})$$

where p_0 is a reference momentum. The χ^2 function above has a minimum for $p = 0$, corresponding to an unphysical solution. Since the momentum is the only degree of freedom, the expectation value of the χ^2 distribution should be 1 and its variance should be 2. The best estimate for a momentum estimation is therefore given by the condition:

$$\chi_{\text{MS},B=0}^2 \stackrel{!}{=} 1. \quad (\text{C.3})$$

One then obtains:

$$p_{\text{MS},B=0} = \frac{p_0}{\sqrt{\boldsymbol{\Psi}^\top \mathbf{D}_{\text{MS}}(p_0) \boldsymbol{\Psi}}}, \quad (\text{C.4})$$

$$\sigma(p)_{\text{MS},B=0}^2 = \frac{2p_0^2}{\boldsymbol{\Psi}^\top \mathbf{D}_{\text{MS}}(p_0) \boldsymbol{\Psi}}. \quad (\text{C.5})$$

The variance, and therefore the precision of the momentum measurement, is inverse proportional to the number of scattering layers (triplets).

The same method can also be used in the presence of hit position errors by using the following replacement:

$$\mathbf{D}_{\text{MS}}(p_0)^{-1} \rightarrow \mathbf{K}^{-1} = \mathbf{D}_{\text{MS}}(p_0)^{-1} + \frac{p^2}{p_0^2} \vec{\mathbf{H}} \vec{\mathbf{D}}_{\text{hit}}^{-1} \vec{\mathbf{H}}^\top \quad (\text{C.6})$$

However, as the momentum determines the relative weight between MS and hit position errors, the solution can only be determined iteratively.

D. Triplet with General Field Configuration

An inhomogeneous or irregular magnetic field represents the greatest challenge for the calculation of the triplet parameters. The main difficulty is that several trajectories connecting the hit positions \vec{x}_0 , \vec{x}_1 , and \vec{x}_2 need to be found, and this by means of track extrapolation since no analytical solution exists.

In the following, an algorithm is presented that finds a reference trajectory for an arbitrary (inhomogeneous) magnetic field by means of track extrapolation. The same algorithm will be used to calculate the fundamental triplet parameters and the hit gradients.

D.1. Finding a Reference Trajectory

In the following, it is assumed that an approximate solution for the hit triplet exists and is known. This could be, for example, a solution obtained under the the assumption of a homogeneous magnetic field using an average magnetic field strength. The reference trajectory can then be found using Newton's method in 2 dimensions ($\vartheta - \varphi$ space). A procedure tailored for hit triplets is described in the following paragraphs.

At the middle hit position, the approximate solution is described by five track parameters:

- $\kappa^{(0)}$: 3D curvature of the approximate trajectory;

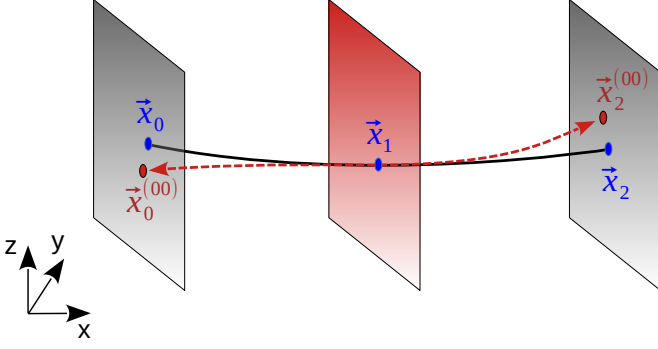


Figure D.11: Sketch showing the first step of the extrapolation algorithm for inhomogeneous magnetic fields. The *black solid* line is the approximate start solution, the *red dashed* line shows the trajectories extrapolated to both sides from the hit \vec{x}_1 at the middle layer.

- $\theta_{10}^{(0)}$ ($\theta_{12}^{(0)}$): polar angle of the first (second) segment at the middle hit position;
- $\phi_{10}^{(0)}$ ($\phi_{12}^{(0)}$): azimuthal angle of the first (second) segment at the middle hit position¹⁸.

By extrapolating the trajectory from the middle hit position to both sides, as sketched in Figure D.11, the extrapolated hit positions $\vec{x}_0^{(00)}$ and $\vec{x}_2^{(00)}$ are obtained¹⁹. Then, the polar and azimuthal angles are varied by ε_θ and ε_ϕ , respectively, and a new set of angles is obtained for track extrapolations:

$$\left. \begin{aligned} \theta_{1k}^{(1)} &= \theta_{1k}^{(0)} + \varepsilon_\theta \\ \phi_{1k}^{(1)} &= \phi_{1k}^{(0)} + \varepsilon_\phi \end{aligned} \right\} k = 0, 2 \quad (\text{D.1})$$

On both sides of the triplet, two more extrapolations to the tracking planes L0 and L2 are performed. Let $\vec{x}_k^{(10)}$ be the extrapolated points from the polar angle variation and $\vec{x}_k^{(01)}$ the extrapolated points from the azimuthal angle variation, the matching condition reads:

$$\vec{x}_k \stackrel{!}{=} \vec{x}_k^{\text{extrapol}} = \vec{x}_k^{(00)} + \eta_{\theta,k} \frac{\vec{x}_k^{(10)} - \vec{x}_k^{(00)}}{\varepsilon_\theta} + \eta_{\phi,k} \frac{\vec{x}_k^{(01)} - \vec{x}_k^{(00)}}{\varepsilon_\phi}. \quad (\text{D.2})$$

For each side ($k = 0, 2$), a system of three equations with two unknown correction parameters: $\eta_{\theta,k}$ and $\eta_{\phi,k}$ are obtained. The third degree of freedom corresponds to the segment length, which is indirectly determined by the extrapolation procedure.

¹⁸Note that ϕ and θ denote the azimuthal and polar angles of tangents of the trajectory, whereas φ and ϑ (defined in Section 2.1) denote the azimuthal angles of the chords between hits.

¹⁹The first index in the upper brackets refers to the θ variation extrapolation step, and the second index to the ϕ variation extrapolation step.

Above system of equations can be solved by minimising the spatial distance $\|\vec{x}_k - \vec{x}_k^{\text{extrapol}}\|$. Using the short-hand notation:

$$\begin{aligned} \vec{a}_{\theta,k} &:= \vec{x}_k^{(10)} - \vec{x}_k^{(00)}, \\ \vec{a}_{\phi,k} &:= \vec{x}_k^{(01)} - \vec{x}_k^{(00)}, \end{aligned}$$

the solution for each side ($k = 0, 2$) is given by:

$$\begin{pmatrix} \eta_{\theta,k}/\varepsilon_\theta \\ \eta_{\phi,k}/\varepsilon_\phi \end{pmatrix} = \frac{\vec{x}_k - \vec{x}_k^{(00)}}{\vec{a}_{\theta,k}^2 \vec{a}_{\phi,k}^2 - (\vec{a}_{\theta,k} \vec{a}_{\phi,k})^2} \begin{pmatrix} \vec{a}_{\phi,k}^2 \vec{a}_{\theta,k} - (\vec{a}_{\theta,k} \vec{a}_{\phi,k}) \vec{a}_{\phi,k} \\ \vec{a}_{\theta,k}^2 \vec{a}_{\phi,k} - (\vec{a}_{\theta,k} \vec{a}_{\phi,k}) \vec{a}_{\theta,k} \end{pmatrix}. \quad (\text{D.3})$$

In case of non-linearities, the matching condition might not be fulfilled in one extrapolation step and the procedure needs to be iterated until $\eta_{\theta,k}$ and $\eta_{\phi,k}$ are determined with the required accuracy, i.e., $\|\vec{x}_k - \vec{x}_k^{\text{extrapol}}\| < \text{accuracy}$.

Finally, the track parameters for the reference solution at the middle layer are given by:

$$\theta_{1k} = \theta_{1k}^{(0)} + \eta_{\theta,k} \quad (\text{D.4})$$

$$\phi_{1k} = \phi_{1k}^{(0)} + \eta_{\phi,k}. \quad (\text{D.5})$$

D.2. Determination of the Triplet Parameters

For the determination of the ρ parameters, the curvature is varied according to:

$$\kappa^{(1)} = \kappa^{(0)} + \varepsilon_\kappa \quad (\text{D.6})$$

Using the so modified curvature, the trajectory is extrapolated again from the middle layer to both sides. Similar to the procedure described in Section D.1, a new set of polar $\theta_{1k}^{(\varepsilon_\kappa)}$ and azimuthal $\phi_{1k}^{(\varepsilon_\kappa)}$ angles is determined such that both reconstructed track segments match the actual hit positions. The four fundamental triplet parameters are then obtained from:

$$\rho_\Theta = \frac{\theta_{12}^{(\varepsilon_\kappa)} - \theta_{10}^{(\varepsilon_\kappa)} - \theta_{12} + \theta_{10}}{\varepsilon_\kappa}, \quad (\text{D.7})$$

$$\rho_\Phi = \frac{\phi_{12}^{(\varepsilon_\kappa)} - \phi_{10}^{(\varepsilon_\kappa)} - \phi_{12} + \phi_{10}}{\varepsilon_\kappa}, \quad (\text{D.8})$$

$$\tilde{\Theta}_0 = -\rho_\Theta \kappa^{(0)} + \theta_{12} - \theta_{10}, \quad (\text{D.9})$$

$$\tilde{\Phi}_0 = -\rho_\Phi \kappa^{(0)} + \phi_{12} - \phi_{10}. \quad (\text{D.10})$$

D.3. Determination of the Hit Gradients

For the determination of the hit gradients (see Section 2.2), no further track extrapolations are required. By solving Equation D.2 for the in total 3×3 1σ hit position shifts, a set of nine polar and azimuthal angle shifts is obtained, which serves as input for the calculation of the hit gradients according to Equation 14 and 15.

To summarize, for the determination of the triplet parameters, at least four track extrapolations are needed for

each of the two triplet segments: one for the starting trajectory, two for the determination of the reference trajectory, and one for the curvature variation. In case of large non-linearities, more extrapolations might be required to determine the reference trajectory. This method is universal and can be used for any tracking detector with any arbitrary field configuration.

E. Strip Detectors

In this section, the local triplet fit is discussed for a barrel-type strip detector in a homogeneous magnetic field. In the context of the triplet fit, a detector is defined to be a strip detector if large hit position errors in one detector direction create an additional rotational uncertainty of the triplet that cannot not be neglected. This rotational degree of freedom is caused by the hit position dependence of the triplet parameters that has been neglected in Section 3 and Section 4.

Here, only the configuration with strips oriented in axial direction is considered, which is used in many experiments. Since $\sigma_z \gg \sigma_\phi$, such a detector is not able to precisely measure the polar angle. This, however, affects the 3D curvature via the relation $\kappa = \kappa_\perp \sin \vartheta$.

Using the approximation $\Gamma_{\Theta\Theta} \gg \sigma_{\text{MS}}^2$ and $\Gamma_{\Theta\Theta} \gg \Gamma_{\Phi\Phi}$, Equation 45 and following simplifies to:

$$\kappa_{z\text{-strip}} \approx -\frac{\tilde{\Phi}_0}{\rho_\Phi} + \Delta\kappa_{\text{rot}}, \quad (\text{E.1})$$

$$\sigma_{\kappa,z\text{-strip}}^2 \approx \frac{\Gamma_{\Phi\Phi}^*}{\rho_\Phi^2} + \Delta\sigma_{\kappa,\text{rot}}^2, \quad (\text{E.2})$$

$$\chi_{z\text{-strip}}^2 \approx \frac{\tilde{\Theta}_0^2}{\Gamma_{\Theta\Theta}}, \quad (\text{E.3})$$

where additional correction term are added to account for the rotational uncertainty. They are calculated as:

$$\Delta\kappa_{\text{rot}} = -\frac{\tilde{\Phi}_0}{\rho_\Phi} \Delta\vartheta_{\text{rot}} \cot \hat{\vartheta}, \quad (\text{E.4})$$

$$\Delta\sigma_{\kappa,\text{rot}}^2 = \kappa_{z\text{-strip}}^2 \sigma_{\vartheta_{\text{rot}}}^2 \cot^2 \hat{\vartheta}, \quad (\text{E.5})$$

and depend on the triplet rotation and its error:

$$\Delta\vartheta_{\text{rot}} = \frac{\tilde{\Theta}}{2\Gamma_{\Theta\Theta}} (\sigma_2 h_{\Theta,2} - \sigma_0 h_{\Theta,0}), \quad (\text{E.6})$$

$$\sigma_{\vartheta_{\text{rot}}}^2 = \frac{1}{4} (\sigma_0^2 h_{\Theta,0}^2 + \sigma_2^2 h_{\Theta,2}^2). \quad (\text{E.7})$$

Note that triplet rotation and its error are obtained by propagating the hit position shifts and errors through the triplet parameters.

Alternatively, the curvature can also be calculated using the fitted hit positions as input for a second fit.

References

[1] R. E. Kálmán, A new approach to linear filtering and prediction problems, *J. Basic Eng.* 82 (1) (1960) 35.

doi:10.1115/1.3662552.
 URL <http://FluidsEngineering.asmedigitalcollection.asme.org/article.aspx?articleid=1430402>

[2] R. Fruhwirth, Application of Kalman filtering to track and vertex fitting, *Nucl. Instrum. Meth. A* 262 (1987) 444–450. doi:10.1016/0168-9002(87)90887-4.

[3] R. Mankel, Pattern recognition and event reconstruction in particle physics experiments, *Rept. Prog. Phys.* 67 (2004) 553. arXiv:physics/0402039, doi:10.1088/0034-4885/67/4/R03.

[4] V. Blobel, A new fast track-fit algorithm based on broken lines, *Nucl. Instrum. Meth. A* 566 (2006) 14–17. doi:10.1016/j.nima.2006.05.156.

[5] C. Kleinwort, General Broken Lines as advanced track fitting method, *Nucl. Instrum. Meth. A* 673 (2012) 107–110. arXiv:1201.4320, doi:10.1016/j.nima.2012.01.024.

[6] V. Blobel, Software alignment for tracking detectors, *Nucl. Instrum. Meth. A* 566 (2006) 5–13. doi:10.1016/j.nima.2006.05.157.

[7] V. Blobel, C. Kleinwort, F. Meier, Fast alignment of a complex tracking detector using advanced track models, *Comput. Phys. Commun.* 182 (2011) 1760–1763. arXiv:1103.3909, doi:10.1016/j.cpc.2011.03.017.

[8] N. Berger, A. Kozlinskiy, M. Kiehn, A. Schöning, “A new three-dimensional track fit with multiple scattering”, *Nucl. Instrum. Methods Phys. Res. A: Accelerators, Spectrometers, Detectors and Associated Equipment* 844 (2017) 135 – 140. doi:https://doi.org/10.1016/j.nima.2016.11.012.

[9] K. Arndt, et al., “Technical design of the phase I Mu3e experiment”, *Nucl. Instrum. Meth. A* 1014 (2021) 165679. arXiv:2009.11690, doi:10.1016/j.nima.2021.165679.

[10] A. Kozlinskiy, Track reconstruction for the Mu3e experiment based on a novel Multiple Scattering fit, *EPJ Web Conf.* 150 (2017) 00005. doi:10.1051/epjconf/201715000005.

[11] D. vom Bruch, Online Data Reduction using Track and Vertex Reconstruction on GPUs for the Mu3e Experiment, *EPJ Web Conf.* 150 (2017) 00013. doi:10.1051/epjconf/201715000013.

[12] A. Schöning, A New Track Reconstruction Algorithm suitable for Parallel Processing based on Hit Triplets and Broken Lines, *EPJ Web Conf.* 127 (2016) 00015. doi:10.1051/epjconf/201612700015.

[13] V. L. Highland, “Some practical remarks on multiple scattering”, *Nucl. Inst. & Meth. A* 129 (1975) 497–499. doi:10.1016/0029-554X(75)90743-0.

[14] G. R. Lynch, O. I. Dahl, Approximations to multiple Coulomb scattering, *Nucl. Instrum. Meth. B* 58 (1991) 6–10. doi:10.1016/0168-583X(91)95671-Y.

[15] D. Colella, ALICE ITS upgrade for LHC Run 3: commissioning in the laboratory, *J. Phys. Conf. Ser.* 2374 (1) (2022) 012058. arXiv:2106.16168, doi:10.1088/1742-6596/2374/1/012058.

[16] B. Abelev, et al., Technical Design Report for the Upgrade of the ALICE Inner Tracking System, *J. Phys. G* 41 (2014) 087002. doi:10.1088/0954-3899/41/8/087002.

[17] ATLAS Collaboration, “Technical Design Report for the ATLAS ITk Pixel Detector”, *Tech. Rep. ATL-COM-ITK-2018-019*, CERN, Geneva (Mar 2018). URL <https://cds.cern.ch/record/2310230>

[18] G. Aglieri Rinella, The ALPIDE pixel sensor chip for the upgrade of the ALICE Inner Tracking System, *Nucl. Instrum. Meth. A* 845 (2017) 583–587. doi:10.1016/j.nima.2016.05.016.

[19] R. Frühwirth, A. Strandlie, *Pattern Recognition, Tracking and Vertex Reconstruction in Particle Detectors*, Particle Acceleration and Detection, Springer, 2020. doi:10.1007/978-3-030-65771-0.